Title	Characterization of cooperative bicarbonate uptake into chloroplast stroma in the green alga Chlamydomonas reinhardtii.
Author(s)	Yamano, Takashi; Sato, Emi; Iguchi, Hiro; Fukuda, Yuri; Fukuzawa, Hideya
Citation	Proceedings of the National Academy of Sciences of the United States of America (2015)
Issue Date	2015-05-26
URL	http://hdl.handle.net/2433/198148
Right	© 2015 National Academy of Sciences
Type	Journal Article
Textversion	author

Classification: BIOLOGICAL SCIENCES: Plant Biology

Title: Characterization of cooperative bicarbonate uptake into chloroplast stroma in the green alga *Chlamydomonas reinhardtii*

Short title: Cooperative bicarbonate uptake

Authors: Takashi Yamano, Emi Sato, Hiro Iguchi, Yuri Fukuda, Hideya Fukuzawa

Author affiliation: Graduate School of Biostudies, Kyoto University, Kyoto, 606-8502, Japan

Corresponding author: Hideya Fukuzawa

Graduate School of Biostudies, Kyoto University, Kyoto, 606-8502, Japan

Phone: +81-75-753-6277

E-mail: fukuzawa@lif.kyoto-u.ac.jp

Keywords: bicarbonate uptake, *Chlamydomonas*, chloroplast envelope, CO_2-concentrating mechanism, photosynthesis

ABSTRACT

The supply of inorganic carbon (Ci; CO_2 and HCO_3^-) is an environmental rate-limiting factor in aquatic photosynthetic organisms. To overcome the difficulty in acquiring Ci in limiting-CO_2 conditions, an active Ci uptake system called the CO_2-concentrating mechanism (CCM) is induced to increase CO_2 concentrations in the chloroplast stroma. An ATP-binding cassette transporter, HLA3, and a formate/nitrite transporter homolog, LCIA, are reported to be associated with HCO_3^- uptake [Wang and Spalding (2014) *Plant Physiol* 166(4):2040–2050]. However, direct evidence of the route of HCO_3^- uptake from the outside of cells to the chloroplast stroma remains elusive owing to a lack of information on HLA3 localization and comparative analyses of the contribution of HLA3 and LCIA to the CCM. In this study, we revealed that HLA3 and LCIA are localized to the plasma membrane and chloroplast envelope, respectively. Insertion mutants of *HLA3* and/or *LCIA* showed decreased Ci affinities/accumulation, especially in alkaline conditions where HCO_3^- is the predominant form of Ci. HLA3 and LCIA formed protein complexes independently, and the absence of LCIA decreased *HLA3* mRNA accumulation, suggesting the presence of unidentified retrograde signals from the chloroplast to the nucleus to maintain *HLA3* mRNA expression. Furthermore, although single overexpression of HLA3 or LCIA in high CO_2 conditions did not affect Ci affinity, simultaneous overexpression of HLA3 with LCIA significantly increased Ci affinity/accumulation. These results highlight the HLA3/LCIA-driven cooperative uptake of HCO_3^- and a key role of LCIA in the maintenance of HLA3 stability as well as Ci affinity/accumulation in the CCM.

Significance Statement

The entry of inorganic carbon (Ci; CO_2 and HCO_3^-) into cells involves many biological processes in both animals and plants, and aquaporins as well as bicarbonate transporters play roles in Ci transport. Although transporting external HCO_3^- into the stroma through the chloroplast envelope is one of the rate-limiting factors for aquatic photosynthetic organisms, specific molecular components in this process have not yet been identified experimentally. Molecular identification of proteins essential for Ci uptake located in the chloroplast envelope as well as in the plasma membrane documented in this study helps in understanding how aquatic photosynthetic organisms developed machinery to acclimate to CO_2-limiting environment and to maintain adequate levels of photosynthesis for survival or growth.

Introduction

Inorganic carbon (Ci; CO_2 and HCO_3^-) transport is essential for a wide range of biological processes such as CO_2 metabolism, cellular pH homeostasis, and photosynthesis. Because HCO_3^- is not freely permeable to biological membranes, it must be transported across membranes by HCO_3^- transporters or channels. HCO_3^- transporters have been studied extensively in mammals and been found to cluster into solute carrier (SLC) 4 and SLC 26 families (1). In cyanobacteria, five types of Ci transporters have been identified (2), including three HCO_3^- transporters and two NAD(P)H dehydrogenase-dependent CO_2 uptake systems. In land plants aquaporin-mediated CO_2 permeation has been suggested to play physiological roles in photosynthesis (3), and in a marine diatom SLC4 family protein localized to the plasma membrane (PM) facilitates HCO_3^- uptake (4). However, no studies have validated the entire route of HCO_3^- transport from the outside of cells to the chloroplast stroma through the PM and chloroplast envelope (CE) in photosynthetic organisms.

Aquatic conditions are not well suited for efficient photosynthesis because the CO_2 diffusion rate is approximately 10,000-fold lower compared with that in atmospheric conditions (5). Therefore, aquatic photosynthetic organisms, including microalgae, are frequently exposed to limiting CO_2 stress. To acclimate to this stress, most microalgae possess a CO_2-concentrating mechanism (CCM) to accumulate CO_2 around the CO_2-fixation enzyme ribulose 1, 5-bisphosphate carboxylase/oxygenase (Rubisco) and to maintain adequate photosynthetic efficiency (6, 7).

The green alga *Chlamydomonas reinhardtii* has been used as a model organism for molecular and physiological studies of the CCM since it was first identified (8). A model of the CCM has been proposed based on the subcellular structure of *C. reinhardtii* (9, 10). Environmental Ci is transported to the chloroplast stroma by Ci transporters localized to the PM and CE. Carbonic anhydrase (CA) localized to the chloroplast stroma is predicted to contribute to the maintenance of the Ci pool, in the form of HCO_3^-, by rapid conversion of CO_2 to HCO_3^-, thereby preventing the loss of CO_2 by diffusion (11). It is known that tubule-like thylakoid membranes penetrate into the pyrenoid (12), a Rubisco-enriched structure in the chloroplast. HCO_3^- in the stroma is transported into the acidic thylakoid lumen by a putative channel or transporter localized to the thylakoid membrane, and HCO_3^- is rapidly converted to CO_2 by a

4

constitutively expressed CA (13, 14). Then, CO_2 diffuses from the thylakoid lumen into the pyrenoid matrix and is fixed by Rubisco. It was also reported that *C. reinhardtii* acclimates to two distinct limiting-CO_2 conditions, termed low-CO_2 (LC; ~0.03–0.5% CO_2 or 7–70 μM CO_2) and very-low-CO_2 (VLC; <0.02% CO_2 or <7 μM CO_2) (15, 16), and different types of Ci uptake systems could function in the CCM in these separate conditions (16).

To identify CCM-associated components, several transcriptome analyses have been performed (17–22), and several genes encoding membrane proteins were focused on as candidate Ci transporter genes, including *LCI1* (low CO_2 inducible gene 1) (23), *LCIA* (low CO_2 inducible gene A) (19), and *HLA3* (high light activated 3) (24).

LCI1 is localized to the PM (25), and its expression is regulated by the MYB-transcription factor LCR1 (low CO_2 stress response 1) (26). When *LCI1* was artificially expressed in HC conditions, the cells showed increases in the internal Ci pool, suggesting that LCI1 is directly or indirectly associated with Ci uptake (25). LCIA (also known as NAR1.2) is a homolog of the nitrate transporter NAR1 and belongs to the formate/nitrite transporter family (27). Although the expression of other *NAR1* family genes of *C. reinhardtii* is mainly regulated by nitrogen source, *LCIA* is specifically induced in LC conditions and is not under the control of nitrogen source (19). LCIA was predicted to localize to the CE (19), and this prediction was supported by indirect immunofluorescence assay evidence (16). Functional expression analysis using *Xenopus* oocytes showed transport activity of LCIA for both HCO_3^- and NO_2^- (27), and LCIA appears to be associated with HCO_3^- uptake in VLC conditions from analysis of an insertion mutant (16). HLA3 is an ATP-binding cassette (ABC) transporter of the multidrug-resistance-related protein subfamily, and its transcription is induced by high light as well as LC conditions (19, 24). Although HLA3 is predicted to localize to the PM (10), no experimental data is available at present. Knockdown (KD) of *HLA3* mRNA expression resulted in modest decreases in photosynthesis affinity, but simultaneous KD of *LCIA* and *HLA3* mRNAs caused a dramatic decrease in growth rate, Ci uptake activity, and photosynthetic Ci affinity, especially in alkaline conditions, where HCO_3^- is the predominant form of Ci (28).

In this study, by use of indirect immunofluorescence assays and membrane fractionation, the subcellular localization of HLA3 was elucidated. In addition, by

analyses of the photosynthetic characteristics of *HLA3* and *LCIA* single insertion mutants, an *HLA3*/*LCIA* double insertion mutant, and overexpressing strains of *HLA3* and/or *LCIA*, we concluded that HLA3 and LCIA are cooperatively associated with HCO_3^- uptake across the PM and CE, respectively.

Results

Accumulation of HLA3 and LCIA in Very-Low-CO_2 Conditions

First, to define the acclimated states of limiting CO_2 conditions (LC or VLC) of cells grown in liquid culture, total Ci concentration in the culture medium at pH 7.0 was measured and consequent CO_2 concentrations were calculated (Fig. 1*A*). CO_2 concentrations supplied with 0.04% CO_2 for 1, 2, 4, 6, and 12 h were estimated as 6.3, 3.1, 2.9, 1.9, and 1.8 μM, respectively, which correspond to the range for VLC (<7 μM CO_2) (16). Thus, we defined the limiting CO_2 conditions of liquid culture as VLC throughout this study. Next, the time course accumulation of HLA3 and LCIA after VLC induction was examined (Fig. 1*A*). The accumulation of these proteins started within 1 h and reached their maximum levels within 4 h, as was the case for LCI1 used as a control of VLC induction. The molecular masses of HLA3 and LCIA were detected at sizes of ~133 kDa and 27 kDa, respectively (Fig. S1*A* and *SI Results and Discussion*).

Subcellular Localization of HLA3 and LCIA

To analyze the subcellular localization of HLA3, an indirect immunofluorescence assay was performed (Fig. 1*B*). Fluorescence signals from an anti-HLA3 antibody were detected peripherally, suggesting the localization of HLA3 to the PM. Fluorescence signals from an anti-LCIA antibody were detected as a single cup-shaped structure (Fig. 1*B*), as in the previous study (16). To further clarify the localization of HLA3 and LCIA biochemically, protein samples from total cell, PM, and CE fractions were probed with antibodies against HLA3, LCI1, H^+-ATPase, LCIA, and CCP1 (Fig. 1*C* and *SI Results and Discussion*). LCI1 and H^+-ATPase were enriched in the PM fraction, consistent with the PM localization of these proteins (25, 29). Similarly, a notable enrichment of HLA3 was observed in the PM fraction. LCIA was highly enriched in the CE fraction, where CE protein CCP1 (30) was also enriched. From these results, we concluded that HLA3 and LCIA were localized to the PM and CE, respectively.

6

Isolation of an *HLA3* Insertion Mutant and Photosynthetic Characteristics

To evaluate the degree of contribution of HLA3 to the CCM, we isolated an *HLA3* insertion mutant from our paromomycin resistance gene-tagged mutant library by PCR-based screening, as described previously (31), and designated the strain Hin-1 (Fig. S2*A–C* and *SI Results and Discussion*).

Next, the photosynthetic characteristics were evaluated by measuring the rates of Ci-dependent O_2 evolution of WT, Hin-1, and the complemented strain Hin-1C grown in VLC at different pH. $K_{0.5}$ (Ci) values, the Ci concentration required for half maximal O_2-evolving activity, of WT and Hin-1 were similar at pH 6.2 (ratio of HCO_3^-:CO_2 = 0.7:1) and pH 7.8 (HCO_3^-:CO_2 = 28:1), indicating that the difference in photosynthetic Ci affinity between WT and Hin-1 was not significant (Fig. 2*A*). Because *HLA3* KD strains showed retarded growth rates at pH 9.0 (28) where the ratio of HCO_3^-:CO_2 = 446:1 and HCO_3^- was the predominant form of Ci, we evaluated the changes in Ci affinity during acclimation to VLC at pH 9.0 in a time-course analysis (Fig. 2*B*). Both WT and Hin-1 showed a gradual decrease in $K_{0.5}$ (Ci) during acclimation to VLC. However, although WT in VLC at 6 h showed almost the same Ci affinity compared with that at 12 h (241 ± 87 μM at 6 h and 290 ± 50 μM at 12 h), Hin-1 still showed much lower Ci affinity especially at 6 h (691 ± 143 μM at 6 h and 405 ± 57 μM at 12 h), and the decreased Ci affinity was restored in Hin-1C (296 ± 78 μM at 6 h and 333 ± 89 μM at 12 h). These results suggested that other Ci uptake systems could compensate for the absence of HLA3 and contribute to the increase in Ci affinity at 12 h, and that measuring photosynthetic characteristics at 6 h was appropriate for evaluating the contribution of HLA3 to the CCM.

To evaluate the contribution of HLA3 to actual Ci uptake activity, the accumulation and fixation of [^{14}C]-labeled Ci in WT, Hin-1, and Hin-1C grown in VLC for 6 h were measured (Fig. 2*C*). Hin-1 showed significantly lower levels of Ci accumulation of 0.12 mM (0.57-fold of Hin-1C), 0.12 mM (0.32-fold), and 0.06 mM (0.17-fold) after 80, 160, 240 s of illumination, respectively, and CO_2 fixation of 0.37 nmol μL SIS^{-1} (0.59-fold), 0.67 nmol μL SIS^{-1} (0.49-fold), and 0.83 nmol μL SIS^{-1} (0.44-fold), respectively, compared with that of Hin-1C. These results indicated that HLA3 has a meaningful role in HCO_3^- uptake in VLC conditions.

Isolation of *LCIA* Insertion Mutants and Photosynthetic Characteristics

A disruption mutant of *LCIA* has been characterized, and the contribution of LCIA to the CCM has been reported (16). To compare the degrees of the contributions of HLA3 and LCIA to the CCM, we also isolated two *LCIA* insertion mutants (Fig. S2*D–G* and *SI Results and Discussion*), designated as Ain (Ain-1 and Ain-2), and compared the photosynthetic characteristics with Hin-1. Interestingly, accumulation of HLA3 was much lower in Ain compared with that in WT, and this decreased accumulation of HLA3 was restored in the complemented strains Ain-1C and Ain-2C (Fig. 3*A*). This result was in sharp contrast to that of LCI1 and LCIB (32), which were not affected by the impairment of the *LCIA* (Fig. 3*A*).

Next, the photosynthetic characteristics of Ain-1, Ain-2, Ain-1C, and Ain-2C were evaluated. As in the case of Hin-1, the $K_{0.5}$ (Ci) of Ain-1 and Ain-2 was similar to WT at pH 6.2 (Fig. 3B). However, in contrast to Hin-1, the $K_{0.5}$ (Ci) of Ain-1 (57 ± 2 μM at 6 h and 56 ± 3 μM at 12 h) and Ain-2 (57 ± 1 μM at 6 h and 57 ± 2 μM at 12 h) were significantly higher than that of WT (40 ± 3 μM at 6 h and 33 ± 3 μM at 12 h), Ain-1C (38 ± 2 μM at 6 h and 32 ± 2 μM at 12 h), and Ain-2C (37 ± 3 μM at 6 h and 29 ± 2 μM at 12 h) even at pH 7.8 (Fig. 3*B*). At pH 9.0, although Ain also showed gradual decreases in $K_{0.5}$ (Ci) during acclimation to VLC, these cells always showed lower Ci affinity than Hin-1 (Fig. 2*B*) as well as WT and complemented strains (Fig. 3*C*). These results suggested a significant contribution of LCIA to increases in Ci affinity and to maintaining HLA3 stability in the CCM.

Isolation of *LCIA*/*HLA3* Double-Insertion Mutants and Photosynthetic Characteristics

Because Ci affinity in VLC at 12 h was higher than that at 6 h in both *HLA3* and *LCIA* single mutants, either protein could partially complement each other to increase Ci affinity. Thus, we expected that *LCIA*/*HLA3* double-insertion mutants would show an additive decrease in Ci affinity compared with the single-insertion mutants. Thus, we isolated double-insertion mutants by crossing one of the Ain-2 progeny with Hin-1, and designated these as AHin (AHin-1 and AHin-2; Fig. 3*D*, Fig. S2*H–K*, and *SI Results and Discussion*).

Next, the photosynthetic characteristics of AHin-2 were evaluated (Fig. 3*E*). As in the case of Hin-1 and Ain, the $K_{0.5}$ (Ci) of AHin-2 was similar to WT at pH 6.2. At pH 7.8, the $K_{0.5}$ (Ci) of AHin-2 (58 ± 2 μM at 6 h and 61 ± 10 μM at 12 h) was significantly higher than that of WT, but it was similar to Ain. At pH 9.0, AHin-2 showed lower Ci affinity than both Hin-1 and Ain, and Ci affinity was not increased even at 12 h (898 ± 78 μM at 6 h and 901 ± 94 μM at 12 h). Ci accumulation and fixation in AHin-2 grown in VLC at 6 h was also measured (Fig. 3*F*). After 80, 160, and 240 s of illumination, AHin-2 showed substantially decreased Ci accumulation of 0.05 mM (0.21-fold of WT and 0.41-fold of Hin-1), 0.06 mM (0.16-fold and 0.53-fold), and 0.06 mM (0.15-fold and 1.0-fold), respectively, and CO_2 fixation of 0.07 nmol μL SIS^{-1} (0.1-fold and 0.2-fold), 0.12 nmol μL SIS^{-1} (0.08-fold and 0.17-fold), and 0.14 nmol μL SIS^{-1} (0.07-fold and 0.17-fold), respectively, compared with that of WT and Hin-1.

Finally, the effect of absence of LCIA and/or HLA3 on cell growth was examined. Growth rates were measured in VLC at pH 8.4 (Fig. S2*L*) because there were no significant differences at pH 7.8, and none of the cell lines could grow at pH 9.0. The doubling time of WT was 7.2 h and that of Hin-1, Ain-1, Ain-2, and AHin-2 increased significantly to 7.6, 9.5, 9.3, and 12.7 h, respectively, reflecting the degree of decreased Ci affinity of each cell line. These results highlighted an additive decrease in Ci affinity/accumulation/growth rates of the double-insertion mutant compared with the *HLA3* or *LCIA* single-insertion mutants.

Isolation of LCIA and/or HLA3 Overexpressing Strains and Photosynthetic Characteristics

To demonstrate the physiological function of LCIA and HLA3 more directly, the photosynthetic characteristics of cells overexpressing LCIA and/or HLA3 were examined in HC conditions where other VLC-inducible proteins were not induced. For overexpression, two chimeric plasmids, pTY2b-LCIA and pTY2b-HLA3, were constructed (Fig. S3*A*). These plasmids allowed the induction of *LCIA* and *HLA3* transcripts by switching the nitrogen source from NH_4^+ to NO_3^- irrespective of the CO_2 conditions. In this study, we cultured the cells with four combinations of nitrogen

sources in the medium and CO_2 concentrations, designated as HC-NH_4^+, HC-NO_3^-, VLC-NH_4^+, and VLC-NO_3^-.

First, we transformed WT cells with pTY2b-LCIA or pTY2b-HLA3, separately. The transformants showed accumulation of LCIA or HLA3 when grown in HC-NO_3^- conditions, and were designated as Aox (Aox-1 and Aox-2) and Hox (Hox-1 and Hox-2), respectively (Fig. S3*B* and *C* and *SI Results and Discussion*). Next, by introducing pTY2b-HLA3 into Aox-1, we generated two independent transformants expressing LCIA and HLA3 simultaneously and designated these as AHox (AHox-1 and AHox-2) (Fig. S3*D*). Accumulation of HLA3 in AHox-1 and AHox-2 was the same as that of VLC-grown WT. To isolate a strain overexpressing both LCIA and HLA3 with greater abundance, the progeny of Aox-1 was crossed with Hox-1 and a strain designated as AHox-3 was obtained (Fig. S3*E*).

Next, to evaluate the effect of LCIA and/or HLA3 overexpression on the photosynthetic characteristics, rates of O_2-evoluton at pH 6.2, 7.8, and 9.0 and Ci accumulation at pH 9.0 of these strains were measured. In Aox, there were no differences in Ci affinity at pH 7.8 and pH 9.0 as well as Ci accumulation compared with WT (Fig. 4*A* and Table S1–S3). In contrast, HC-NO_3^--grown Hox showed a small but significant increase of Ci accumulation of 0.08 mM (2.5-fold of WT at 80 s), 0.07 mM (1.5-fold at 160 s), and 0.13 mM (2.4-fold at 240 s) in Hox-2, compared with that of HC-NO_3^--grown WT, but the phenotype led to a slight increase in Ci affinity only at pH 9.0 in Hox-2 (Fig. 4*B*), suggesting that Ci in the cytosol transported by HLA3 could not efficiently enter the chloroplast stroma in the absence of LCIA. On the other hand, Ci affinity at pH 6.2 was increased in LCIA-overexpressing Aox (Fig. 4*A*) and AHox (Fig. 4*C*), but not in Hox (Fig. 4*B*).

In contrast to Aox and Hox, AHox showed a significant increase in Ci affinity as well as Ci accumulation compared with WT at alkaline conditions (Fig. 4*C* and Table S2 and S3). In particular, HC-NO_3^--grown AHox-3 showed substantially increased Ci accumulation of 0.21 mM (6.3-fold of WT at 80 s), 0.34 mM (6.8-fold at 160 s), and 0.19 mM (3.6-fold at 240 s) compared with that of HC-NO_3^--grown WT. Consequently, the respective $K_{0.5}$ (Ci) of AHox-1, AHox-2, and AHox-3 decreased to 141 ± 20 (0.61-fold of WT), 174 ± 20 (0.76-fold), and 147 ± 19 μM (0.64-fold) at pH 7.8 and to 1821 ± 201 (0.68-fold of WT), 1980 ± 198 (0.75-fold), and 1626 ± 49 μM (0.61-fold) at

pH 9.0. In HC-NH$_4^+$ conditions at pH 7.8 where *LCIA* and *HLA3* were not induced, the respective K$_{0.5}$ (Ci) of 257 ± 28, 250 ± 30, and 262 ± 29 µM in AHox-1, AHox-2, and AHox-3 were not significantly different from that of 273 ± 31 µM in WT (Table S2). These results indicated that NO$_3^-$-induced overexpression of LCIA and HLA3 could enhance HCO$_3^-$ accumulation in the chloroplast stroma and increase Ci affinity.

Although PM-localized LCI1 could be associated with Ci uptake (25), the preferred Ci species of LCI1 remained elusive. To evaluate the degree of LCIA/HLA3-driven HCO$_3^-$ uptake activity, we also isolated six transformants expressing LCIA with LCI1 by introducing pTY2b-LCI1 (Fig. S3*A*) into Aox-1, and designated two representatives as A1ox (A1ox-1 and A1ox-2) (Fig. S3*F*). There were no differences in Ci accumulation and affinity in alkaline conditions compared with WT (Fig. 4*D* and Table S2 and S3), suggesting that LCI1 was not related to direct HCO$_3^-$ uptake along with LCIA.

A Defect in LCIA Led to a Decrease in HLA3 Accumulation Caused by Suppression of *HLA3* mRNA Accumulation

As described above, accumulation of HLA3 was much lower in Ain compared with that in WT (Fig. 3*A*). This result suggested two possibilities. First, HLA3 and LCIA undergo physical interaction where the PM is associated with the CE and the absence of LCIA causes instability of HLA3. Second, the absence of LCIA causes the repression of *HLA3* mRNA accumulation.

To examine the former possibility, the molecular masses of LCIA and HLA3 *in vivo* were estimated by Blue Native-PAGE. We expected that LCIA and HLA3 should be detected with the same molecular mass in non-denaturing conditions if these two proteins interact and form a complex. However, using 1.0% n-dodecyl β-D-maltoside (DDM) as a detergent, LCIA and HLA3 were detected with different sizes of approximately 240 and 580 kDa, respectively (Fig. 5*A*). We also estimated the molecular masses using different DDM concentrations (0.25%, 0.5%, 1.0%, or 2.0%) or using formaldehyde cross-linker, and still LCIA and HLA3 were detected at 240 and 580 kDa, respectively (Fig. S4*A* and *B*). Furthermore, LCIA and HLA3 could form respective complexes with the same molecular masses even in Aox, Hox, and AHox cells grown in HC-NO$_3^-$ conditions (Fig. S4*C*). These results strongly suggested that

11

LCIA and HLA3 did not interact physically *in vivo* and at least VLC-inducible proteins other than LCIA and HLA3 were not associated with the formation of the respective protein complexes.

For the latter possibility, *HLA3* mRNA accumulation was evaluated by quantitative real-time PCR (Fig. 5*B*). The sequences of primers used are listed in Table S4. *HLA3* mRNA levels were significantly reduced in Ain-1 and Ain-2 grown in VLC, but mRNA accumulation was restored in the complemented strains. In contrast, the mRNA levels of *LCIA* were not affected in Hin-1 (Fig. 5*B*), and those of other VLC-inducible genes *LCIB* and *LCI1* were also largely unchanged in Ain-1 and Ain-2 as well as Hin-1 (Fig. S4*D*). These results suggested that LCIA localized to the CE could affect the mRNA expression level of *HLA3* and subsequently caused a decrease in HLA3 protein accumulation.

Discussion

In this study, by characterizing the photosynthetic phenotype of *LCIA* and *HLA3* insertion/overexpressing strains, it was revealed that HLA3 and LCIA are parts of the mechanism of HCO_3^- uptake through the PM and CE. These results elucidated a route of HCO_3^- uptake from the outside of cells to the chloroplast stroma by the cooperative function of HLA3 and LCIA.

Although LCIA could be associated with HCO_3^- uptake, the molecular mechanism remains elusive. LCIA is a homolog of formate transporter FocA and contains five amino acid residues (Fig. S2*F*) corresponding to those shown to form the pore of FocA (19, 33). FocA forms a symmetric pentamer that closely resembles the structure of aquaporin (33) and facilitates formate transport as a channel. Considering that LCIA was detected at 240 kDa in non-denaturing conditions (Fig. 5*A*), LCIA forms a protein complex as in the case of FocA. Furthermore, considering that the capacity for formate passage by FocA is increased by mutations of the afore mentioned amino acids to smaller residues (33), examining the effect of similar mutations in LCIA could be helpful in elucidating the function of LCIA as a potential HCO_3^- channel. Relating to this hypothesis, a significant increase in Ci affinity at pH 6.2 was observed in LCIA-overexpressing strains (Fig. 4*A*, *C*, and *D*). Considering that external CO_2 at pH 6.2 should enter the cytoplasm continuously by passive influx, LCIA could function as

12

a channel and cause an increase in the apparent Ci conductance with a minimal concentration gradient without waiting for a notable increase in Ci accumulation in the cytoplasm. In contrast, endogenous levels of HLA3 in HC conditions were not sufficient for Ci permeation towards the chloroplast stroma even with increased cytosolic Ci accumulation (Fig. 4*B*). These results suggested the functional importance of LCIA as a bottle neck step for increases in photosynthetic conductance across the CE.

By measuring the Ci accumulation and affinity of LCIA/LCI1-overexpressing strains, the degree of LCIA/HLA3-dirven HCO_3^- uptake activity was evaluated (Fig. 4*D*). However, there were no differences in Ci accumulation and affinity at pH 9.0 compared with WT, suggesting that LCI1 was not related to the direct HCO_3^- uptake along with LCIA. Furthermore, although it was reported that Ci affinity was increased by the single overexpression of LCI1 at pH 7.8 (25), A1ox did not show a significant increase in Ci affinity in the same pH conditions. This discrepancy could be caused by the difference in $K_{0.5}$ (Ci) values of the strains examined. For overexpressing LCI1 in the previous report, strain *lcr1* deficient in mRNA expression for at least three genes, *LCI1*, *CAH1*, and *LCI6* (26) was used and its $K_{0.5}$ (Ci) was 445 ± 38 μM in HC conditions at pH 7.8 (25). In contrast, the $K_{0.5}$ (Ci) of strain C9 used as WT in this study was 230 ± 27 μM in the same conditions, which was almost the same as 245 ± 38 μM when LCI1 was overexpressed in *lcr1* (25). Thus, the effect of overexpressing LCI1 could be masked in A1ox cells.

By means of *LCIA* insertion mutant analyses, it was shown that LCIA localized to the CE affected *HLA3* mRNA expression in the nucleus (Fig. 5*B*), which could throw new light on understanding the regulation of *LCIA* and *HLA3*. Considering that LCIA expression was not affected by the absence of HLA3 (Fig. 5*B*), there may be unidentified retrograde signals from the chloroplast to the nucleus for maintaining HLA3 mRNA expression. This possibility is supported by the recent study showing that transcript levels of LCIA and HLA3 were simultaneously impaired in an HC-requiring mutant containing a disrupted *CAS* gene encoding a putative chloroplast calcium sensor protein and that other LC-inducible genes, such as *CAH1*, *LCI1*, *LCIB*, and *LCIC*, were unaffected in the *CAS* mutant (34). Furthermore, this suggested that LCIA and HLA3 could function cooperatively as part of the CCM and that LCIA has a key role in

guaranteeing the maintenance of the HCO_3^- uptake system. Because LCIA and HLA3 are conserved among aquatic algae, and owing to the structural relationship of LCIA homologs with aquaporin (33), the *LCIA* and *HLA3* genes may have potential for genetic improvement of photosynthesis in land plants as well as algae.

Materials and Methods

C. reinhardtii strain C9 (photosynthetically WT strain available from the National Institute for Environmental Studies, Japan, as strain NIES-2235) was cultured in Tris-acetate-phosphate (TAP) medium for maintenance. For physiological experiments, cells were grown in liquid TAP medium for pre-cultivation and diluted with modified high-salt medium (HSM (NH_4^+)) containing 9.35 mM NH_4Cl supplemented with 20 mM MOPS (pH 7.0) to an OD_{730} of ~0.05 for photoautotrophic growth. To induce the expression of exogenous genes, cells grown in HSM (NH_4^+) medium for ~24 h to an OD_{730} of ~0.3 were collected by centrifugation and resuspended in fresh HSM (NO_3^-) containing 9.35 mM KNO_3 aerated with air enriched with 5% CO_2 (HC) or ordinary air containing 0.04% CO_2 (VLC). The culture conditions with combinations of medium and CO_2 concentrations are described as HC-NH_4^+, HC-NO_3^-, VLC-NH_4^+, and VLC-NO_3^-. For all culture conditions, cells were cultured at 25°C with illumination at 80 μmol photons $m^{-2}\,s^{-1}$.

Additional experimental procedures and methods are listed in the SI Materials and Methods.

Footnotes

Acknowledgments

References

1. Cordat E, Casey JR (2009) Bicarbonate transport in cell physiology and disease. *Biochem J* 417(2):423–439.

2. Price GD, Badger MR, Woodger FJ, Long BM (2008) Advances in understanding the cyanobacterial CO_2-concentrating-mechanism (CCM): functional components, Ci transporters, diversity, genetic regulation and prospects for engineering into plants. *J Exp Bot* 59(7):1441–1461.

3. Uehlein N, Lovisolo C, Siefritz F, Kaldenhoff R (2003) The tobacco aquaporin NtAQP1 is a membrane CO_2 pore with physiological functions. *Nature* 425(6959):734–737.

4. Nakajima K, Tanaka A, Matsuda Y (2013) SLC4 family transporters in a marine diatom directly pump bicarbonate from seawater. *Proc Natl Acad Sci USA* 110(5):1767–1772.

5. Jones HG (1992) Plants and microclimate: *A quantitative approach to environmental plant physiology* Ed 2 (Cambridge University Press Cambridge UK).

6. Badger MR, Price GD (2003) CO_2 concentrating mechanisms in cyanobacteria: molecular components, their diversity and evolution. *J Exp Bot* 54(383):609–622.

7. Giordano M, Beardall J, Raven J (2005) CO_2 concentrating mechanisms in algae: mechanisms, environmental modulation, and evolution. *Annu Rev Plant Biol* 56:99–131.

8. Badger MR, Kaplan A, Berry JA (1980) Internal inorganic carbon pool of *Chlamydomonas reinhardtii*: evidence for a carbon-dioxide concentrating mechanism. *Plant Physiol* 66(3):407–413.

9. Moroney JV, Ynalvez R (2007) Proposed carbon dioxide concentrating mechanism in *Chlamydomonas reinhardtii*. *Eukaryot Cell* 6(8):1251–1259.

10. Spalding MH (2008) Microalgal carbon-dioxide-concentrating mechanisms: *Chlamydomonas* inorganic carbon transporters. *J Exp Bot* 59(7):1463–1473.

11. Moroney JV, et al. (2011) The carbonic anhydrase isoforms of *Chlamydomonas reinhardtii*: intracellular location, expression, and physiological roles. *Photosynth Res* 109(1–3):133–149.

12. Ohad I, Siekevitz P, Palade GE (1967) Biogenesis of chloroplast membranes. I. Plastid dedifferentiation in a dark-grown algal mutant (*Chlamydomonas reinhardi*).

J Cell Biol 35(3):521–552.

13. Karlsson J, et al. (1998) A novel alpha-type carbonic anhydrase associated with the thylakoid membrane in *Chlamydomonas reinhardtii* is required for growth at ambient CO_2. *EMBO J* 17(5):1208–1216.

14. Raven JA (1997) Putting the C in phycology. *Eur J Phycol* 32(4):319–333.

15. Vance P, Spalding MH (2005) Growth, photosynthesis, and gene expression in *Chlamydomonas* over a range of CO_2 concentrations and CO_2/O_2 ratios: CO_2 regulates multiple acclimation states. *Can J Bot* 83(7):796–809.

16. Wang Y, Spalding MH (2014) Acclimation to very low CO_2: contribution of limiting CO_2 Inducible proteins, LCIB and LCIA, to inorganic carbon uptake in *Chlamydomonas reinhardtii*. *Plant Physiol* 166(4):2040–2050.

17. Fukuzawa H, et al. (2001) *Ccm1*, a regulatory gene controlling the induction of a carbon-concentrating mechanism in *Chlamydomonas reinhardtii* by sensing CO_2 availability. *Proc Natl Acad Sci USA* 98(9):5347–5352.

18. Xiang Y, Zhang J, Weeks DP (2001) The *Cia5* gene controls formation of the carbon concentrating mechanism in *Chlamydomonas reinhardtii*. *Proc Natl Acad Sci USA* 98(9):5341–5346.

19. Miura K, et al. (2004) Expression profiling-based identification of CO_2-responsive genes regulated by CCM1 controlling a carbon-concentrating mechanism in *Chlamydomonas*. *Plant Physiol* 135(3):1595–1607.

20. Yamano T, Miura K, Fukuzawa H (2008) Expression analysis of genes associated with the induction of the carbon-concentrating mechanism in *Chlamydomonas reinhardtii*. *Plant Physiol* 147(1):340–354.

21. Brueggeman AJ, et al. (2012) Activation of the carbon concentrating mechanism by CO_2 deprivation coincides with massive transcriptional restructuring in *Chlamydomonas reinhardtii*. *Plant Cell* 24(5):1860–1875.

22. Fang W, et al. (2012) Transcriptome-wide changes in *Chlamydomonas reinhardtii* gene expression regulated by carbon dioxide and the CO_2-concentrating mechanism regulator CIA5/CCM1. *Plant Cell* 24(5):1876–1893.

23. Burow MD, Chen ZY, Mouton TM, Moroney JV (1996) Isolation of cDNA clones of genes induced upon transfer of *Chlamydomonas reinhardtii* cells to low CO_2. *Plant Mol Biol* 31(2):443–448.

24. Im CS, Grossman AR (2002) Identification and regulation of high light-induced genes in *Chlamydomonas reinhardtii*. *Plant J* 30(3):301–313.

25. Ohnishi N, et al. (2010) Expression of a low CO_2-inducible protein, LCI1, increases inorganic carbon uptake in the green alga *Chlamydomonas reinhardtii*. *Plant Cell* 22(9):3105–3117.

26. Yoshioka S, et al. (2004) The novel Myb transcription factor LCR1 regulates the CO_2-responsive gene *Cah1*, encoding a periplasmic carbonic anhydrase in *Chlamydomonas reinhardtii*. *Plant Cell* 16(6):1466–1477.

27. Mariscal V, et al. (2006) Differential regulation of the *Chlamydomonas Nar1* gene family by carbon and nitrogen. *Protist* 157(4):421–433.

28. Duanmu D, Miller AR, Horken KM, Weeks DP, Spalding MH (2009) Knockdown of limiting-CO_2-induced gene *HLA3* decreases HCO_3^- transport and photosynthetic Ci affinity in *Chlamydomonas reinhardtii*. *Proc Natl Acad Sci USA* 106(14):5990–5995.

29. Norling B, Nurani G, Franzen LG (1996) Characterization of the H^+-ATPase in plasma membranes isolated from the green alga *Chlamydomonas reinhardtii*. *Physiol Plant* 97(3):445–453.

30. Ramazanov Z, Mason CB, Geraghty AM, Spalding MH, Moroney JV (1993) The low CO_2-inducible 36-kilodalton protein is localized to the chloroplast envelope of *Chlamydomonas reinhardtii*. *Plant Physiol* 101(4):1195–1199.

31. Gonzalez-Ballester D, et al. (2011) Reverse genetics in *Chlamydomonas*: a platform for isolating insertional mutants. *Plant Methods* 7:24.

32. Yamano T, et al. (2010) Light and low-CO_2-dependent LCIB-LCIC complex localization in the chloroplast supports the carbon-concentrating mechanism in *Chlamydomonas reinhardtii*. *Plant Cell Physiol* 51(9):1453–1468.

33. Wang Y, et al. (2009) Structure of the formate transporter FocA reveals a pentameric aquaporin-like channel. *Nature* 462(7272):467–472.

34. Wang L, Yamano T, Kajikawa M, Hirono M, Fukuzawa H (2014) Isolation and characterization of novel high-CO_2-requiring mutants of *Chlamydomonas reinhardtii*. *Photosynth Res* 121(2-3):175–184.

Figure Legends

Fig. 1. Accumulation and subcellular localization of HLA3 and LCIA. (*A*) Time-course of accumulation of HLA3, LCIA, and LCI1 proteins in WT cells. For induction of limiting-CO_2 conditions, cells supplied with 5% (high CO_2; HC) were centrifuged, suspended in new fresh medium, and cultured with 0.04% CO_2 for 1, 2, 4, 6, and 12 h. Histone H3 was used as a loading control. The total Ci concentrations and calculated CO_2 concentrations after each induction time are also indicated below the figures. Using an HCO_3^-/CO_2 ratio of 4.47 at pH 7.0, CO_2 concentrations were calculated using the equation $\{pH = pKa + \log_{10} [HCO_3^-]/[CO_2]\}$, where pKa was an acid dissociation constant of 6.35. (*B*) Subcellular localization of HLA3 and LCIA by an indirect immunofluorescence assay. WT cells were grown in very low CO_2 (VLC) for 12 h. DIC, differential interference contrast; scale bars, 5 μm. (*C*) Immunoblot analysis in isolated plasma membrane (PM) and chloroplast envelope (CE) fractions with antibodies against HLA3, LCI1, H^+-ATPase, LCIA, and CCP1. Asterisks indicate nonspecific bands.

Fig. 2. Characterization of an *HLA3* insertion mutant. (*A*) Inorganic carbon (Ci) affinity of WT and *HLA3* insertion mutant (Hin-1) grown in very low CO_2 (VLC) for 6 h or 12 h. Photosynthetic O_2-evolving activity was measured with different external Ci concentrations at pH 6.2 or 7.8, and the respective $K_{0.5}$ (Ci) values, the Ci concentration required for half maximum O_2-evolving activity, were calculated. (*B*) Ci affinity of WT, Hin-1, and complemented Hin-1 (Hin-1C) grown in high CO_2 (HC) or VLC for 1, 2, 4, 6, and 12 h. O_2-evolving activity was measured at pH 9.0. *$P<0.01$ and **$P<0.05$ by Student's t test. (*C*) Accumulation and fixation of Ci in WT, Hin-1, and Hin-1C. Cells were grown in VLC for 6 h, and intracellular Ci accumulation (*Left*) and CO_2 fixation (*Right*) at pH 9.0 were measured using a silicone-oil layer method. SIS, sorbitol impermeable space.

Fig. 3. Characterization of *LCIA* insertion mutants and an *LCIA*/*HLA3* double-insertion mutant. (*A*) Accumulation of LCIA, HLA3, LCI1, and LCIB in WT, *LCIA* insertion mutants (Ain-1 and Ain-2), and their complemented strains (Ain-1C and Ain-2C). Cells were grown in very low CO_2 (VLC) for 12 h. (*B*) Inorganic carbon (Ci) affinity of WT, Ain-1, Ain-2, Ain-1C, and Ain-2C grown in VLC for 6 h or 12 h. Photosynthetic

O_2-evolving activity was measured with different external Ci concentrations at pH 6.2 or 7.8, and the respective $K_{0.5}$ (Ci) values, the Ci concentration required for half maximum O_2-evolving activity, were calculated. *$P<0.01$. (*C*) Ci affinity of WT, Ain-1, Ain-2, Ain-1C, and Ain-2C grown in high CO_2 (HC) or VLC for 1, 2, 4, 6, and 12 h. O_2-evolving activity was measured at pH 9.0. *$P<0.01$. (*D*) Accumulation of HLA3 and LCIA in WT and *LCIA/HLA3* double-insertion mutants (AHin-1 and AHin-2) grown in VLC for 12 h. (*E*) Ci affinity of WT and AHin-2 grown in HC or VLC for 6 h or 12 h. O_2-evolving activity was measured at pH 6.2, 7.8, or 9.0. *$P<0.01$. (*F*) Accumulation and fixation of Ci in WT and AHin-2. Cells were grown in HC or VLC for 6 h, and intracellular Ci accumulation (*Left*) and CO_2 fixation (*Right*) were measured at pH 9.0. SIS, sorbitol impermeable space.

Fig. 4. Characterization of LCIA- and HLA3-overexpressing strains. Accumulation of inorganic carbon (Ci) (*Left*) and Ci affinity (*Right*) in WT and in strains overexpressing LCIA (A), HLA3 (*B*), LCIA/HLA3 (*C*), and LCIA/LCI1 (*D*). Cells were grown in high CO_2 (HC)-NO_3^- for 12 h, and Ci accumulation was measured at pH 9.0. For Ci affinity, O_2-evolving activity of was measured with different external Ci concentrations at pH 6.2, 7.8, or 9.0 and the respective $K_{0.5}$ (Ci) values, the Ci concentration required for half maximum O_2-evolving activity, were calculated. *$P<0.01$ and **$P<0.05$.

Fig. 5. Molecular masses of LCIA and HLA3 in non-denaturing conditions and effect of the absence of LCIA on *HLA3* mRNA accumulation. (*A*) Molecular masses of LCIA and HLA3 in non-denaturing conditions. Total proteins were solubilized using 1.0% n-dodecyl β-D-maltoside and separated by blue-native PAGE. (B) Quantitative real-time PCR analyses of *HLA3* (*Upper*) and *LCIA* (*Lower*) in WT, Ain-1, Ain-2, Ain-1C, Ain-2C, Hin-1, and Hin-1C. These cells were grown in very low CO_2 conditions for 4 h. Expression of each gene was normalized to *CBLP*. Data in all experiments indicate mean value ± SD from three biological replicates. *$P<0.01$.

Supporting Information

SI Results and Discussion

Molecular Sizes and Accumulation of HLA3 and LCIA

The predicted amino acid sequence of HLA3 varies between databases, and all of the deduced molecular mass values are different from the 133-kDa protein detected (Fig. S1*A*). HLA3 is deposited as a 119.7-kDa protein (accession number EDP07736) (1) in GenBank (http://www.ncbi.nlm.nih.gov/genbank/), as a 146.8-kDa protein (gene ID Cre02.g097800.t1.1) in *Chlamydomonas reinhardtii* v5.5 genome database (http://phytozome.jgi.doe.gov/pz/portal.html#!info?alias=Org_Creinhardtii), and it has also been reported as a 118.7-kDa protein (2). These differences in the predicted amino acid sequence of HLA3 were caused by different predictions of the position of the translation start codon and minor differences in internal amino acid sequences. In this study, to overexpress the exogenous gene, we referred to Cre02.g097800.t1.1, which was the longest among the deposited sequences, for amplifying the *HLA3* gene using genomic DNA from WT strain C9 as a template. As a result, the 133-kDa band detected in an HLA3-overexpressing strain was the same as that of endogenous HLA3. Thus, our overexpressed HLA3 was assumed to correspond to the mature HLA3 protein, and the difference between the detected size of 133 kDa and the predicted size of 146.8 kDa in Phytozome could be caused by aberrant mobility or possible processing of HLA3.

Based on the prediction using the ChloroP program (http://www.cbs.dtu.dk/services/ChloroP/), LCIA possesses a conserved chloroplast transit peptide with putative signal cleavage sequences (V/I-X-A) in *C. reinhardtii* (3, 4). The full-length sequence of LCIA of 34.8 kDa is predicted to be cleaved to a mature protein of 27.5 kDa. Thus, the detected protein band estimated as 27 kDa in the immunoblot analysis (Fig. S1*A*) was assumed to correspond to the mature LCIA protein.

As expected from a previous RNA expression analysis (5), HLA3 and LCIA did not accumulate in C16, a CCM1-deficient regulatory mutant (Fig. S1*A*).

Subcellular Localization of HLA3 and LCIA

Similar to the plasma membrane (PM) protein H^+-ATPase, a notable enrichment of HLA3 was observed in the PM fraction (Fig. 1*C*). Although the protein bands of HLA3

and H$^+$-ATPase were highly aggregated because of the enrichment of the PM, these aggregations were resolved by dilution of the samples (Fig. S1*B*). LCIA and HLA3 were not detected in the thylakoid membrane fraction, where thylakoid membrane protein D1 (photosystem II reaction center protein) was enriched (Fig. S1*C*).

Isolation of *HLA3* and *LCIA* Insertion Mutants

In strain Hin-1, the *aphVIII* cassette was inserted into the 10th exon of *HLA3* (Fig. S2*A*), which was confirmed by genomic PCR (Fig. S2*B*). When primer set *HLA3*-R5 and RB1 was used, a product with a size of ~800 bp was found in Hin-1 but not in WT, indicating that the *aphVIII* cassette was inserted in *HLA3* in Hin-1. When primer set *HLA3*-F5 and *HLA3*-R5 was used, the size of the band in Hin-1 was ~3,000 bp, which was larger than the 1,528-bp band in WT. The increase in the size of the PCR product from Hin-1 was ~1,500 bp, which was almost the same as the size of the *aphVIII* cassette (1,534 bp), suggesting that a single *aphVIII* cassette was inserted in *HLA3* in Hin-1. Accumulation of HLA3 was not detected in Hin-1 by immunoblot analysis using an antibody against the C-terminal region of HLA3 (Fig. S2*C*), suggesting that at least the full-length sequence of HLA3 was not accumulated. In contrast, other CCM-related proteins, including at least LCIA, LCI1, and LCIB, accumulated normally. Introducing a full-length PCR copy of *HLA3* expressed from its native promoter could restore HLA3 accumulation (Fig. S2*C*), and the obtained complemented strain was designated as strain Hin-1C.

In strains Ain-1 and Ain-2, the *aphVIII* cassettes were inserted into the 6th exon and 5th exon of *LCIA* (Fig. S2*D*), respectively, and these insertions were confirmed by genomic PCR (Fig. S2*E*). When primer set *LCIA*-F3 and RB1 was used, products with sizes of ~1,000 bp and 200 bp were found in Ain-1 and Ain-2, respectively, but not in WT, indicating that the *aphVIII* cassette was inserted in *LCIA* in Ain-1 and Ain-2. Moreover, when primer set *LCIA*-F3 and *LCIA*-R2 was used, the size of the DNA band in Ain-1 was approximately 2,800 bp, which was larger than the 819-bp band in WT, and no band was detected in Ain-2. The increase in the size of the PCR product from Ain-1 was ~2,000 bp, which was larger than the size of the *aphVIII* cassette (1,534 bp), suggesting that more than one *aphVIII* cassette was inserted. Sequence analysis of the amplified PCR product using primers *LCIA*-F3 and RB1

2

revealed that a partial *aphVIII* cassette was inserted in tandem in addition to a single unit of the *aphVIII* cassette in Ain-1. The insertions of the *aphVIII* cassette were located in a loop between the predicted 5th and 6th transmembrane regions in Ain-1 and in a loop between the predicted 3rd and 4th transmembrane regions in Ain-2 (Fig. S2*F*). Accumulation of LCIA was not detected in Ain-1 or Ain-2 by immunoblot analysis using an antibody against the C-terminal region of LCIA (Fig. 3*A*). By introducing a full-length PCR copy of *LCIA* expressed from its native promoter, it was possible to recover LCIA accumulation (Fig. 3*A*). The complemented strains were designated as Ain-1C and Ain-2C, respectively.

Isolation of *LCIA*/*HLA3* Double-Insertion Mutants

To isolate the *LCIA*/*HLA3* double-insertion mutants, progenies of the *LCIA* insertion mutant were obtained. Because the DNA gel blot analysis using an *aphVIII*-specific probe confirmed the occurrence of two insertions and a single insertion at the *LCIA* loci in Ain-1 and Ain-2, respectively, we used Ain-2 for further analysis (Fig. S2*G*). First, Ain-2 was crossed with WT strain CC-1690 and eight progenies were obtained, and insertion of *aphVIII* and mating type were examined by genomic PCR (Fig. S2*H*). By measuring the $K_{0.5}$ (Ci) values, the Ci concentration required for half maximum O_2-evolving activity (V_{max}), at pH 9.0, all four progenies (B4, B6, B7 and B8) harboring the *aphVIII* cassette showed more than twofold higher $K_{0.5}$ (Ci) than those of WT and CC-1690 (Fig. S2*I* and Table S3), indicating co-segregation of the *aphVIII* insertion into *LCIA* loci with a significant decrease in Ci affinity. Next, progeny B4 was crossed with Hin-1, and seven progenies (D8 died after hatching) were obtained (Fig. S2*J*). Insertion of *aphVIII* into the respective *LCIA* and *HLA3* loci was examined by genomic PCR, and *LCIA*/*HLA3* double-insertion mutants (D1 and D4), subsequently designated as AHin-1 and AHin-2, were obtained (Fig. S2*K*). As expected, accumulation of LCIA and HLA3 was not detected in AHin-1 and AHin-2 (Fig. 3*D*).

Evaluation of the Overexpression Levels of LCIA and HLA3

Aox-1 and Hox-1 showed strong accumulation of LCIA and HLA3, and their accumulation levels were over 128 and 32 times those in VLC-grown WT cells, respectively (Fig. S3B and C). The accumulation levels of LCIA and HLA3 in Aox-2

and Hox-2 cells were the same as those of LC-grown WT. As in the case of VLC-grown WT cells, peripheral and cup-shaped fluorescence signals corresponding to the plasma membrane (PM) and chloroplast envelope (CE), respectively, were observed in Hox-1 and Aox-1 cells grown in HC-NO_3^- conditions (Fig. S1D).

Photosynthetic Characteristics of Overexpressing Strains

Ci affinity at pH 6.2 was increased in LCIA-overexpressing Aox and AHox, but not in Hox (Fig. 4), supporting the idea that external CO_2 at pH 6.2 should enter the cytosolic space by passive influx, be partially converted to HCO_3^-, and efficiently enter into the chloroplast stroma by support of the overexpressed LCIA. However, there were no significant differences in Ci affinity between Ain and WT cells at pH 6.2 (Fig. 3B). This phenotype has at least two potential explanations. First, other VLC-inducible transporters/channels for increasing Ci conductance at the CE could compensate for the absence of LCIA. This possibility is supported by the finding that the difference in Ci affinity between Ain and WT was not especially different at pH 7.8 (Fig. 3B) and that a gradual increase in Ci affinity was also observed even at pH 9.0 (Fig. 3C). Second, conversion rates between HCO_3^- and CO_2 could be slow in the cytoplasm and a certain amount of unconverted CO_2 could enter into the chloroplast stroma across the CE passively, increasing the Ci affinity in Ain. This possibility is supported by a previous report that the expression of carbonic anhydrase 9, which was predicted to localize to the cytoplasm, can barely be detected in CO_2-limiting conditions (6).

Furthermore, although the increases in Ci affinity, Ci uptake/accumulation, and CO_2 fixation in AHox were apparent (Fig. 5C), VLC-grown WT with an entire set of CCM-related proteins showed much higher Ci affinity than that in AHox. Recent studies showed that post-translational regulation and/or modification of CCM components after switching from HC to limiting CO_2 conditions were important for producing a fully functional CCM, and such modifications may not have occurred in AHox in the conditions tested. For example, localization of the LCIB/LCIC complex proposed for Ci-recycling (7–9) or CO_2 transport (10) changes in response to light conditions and CO_2 concentrations (9). The activation of CAH3, a CA localized to the thylakoid lumen, is also caused by limiting-CO_2-induced phosphorylation (11). Therefore, along with the contribution of Ci transporters including LCIA and HLA3, the

4

regulation of other CCM components could be needed for full activity of the CCM.

1. Merchant SS, et al. (2007) The *Chlamydomonas* genome reveals the evolution of key animal and plant functions. *Science* 318(5848):245–250.

2. Im CS, Grossman AR (2002) Identification and regulation of high light-induced genes in *Chlamydomonas reinhardtii. Plant J* 30(3):301–313.

3. Franzén LG, Rochaix JD, von Heijne G (1990) Chloroplast transit peptides from the green alga *Chlamydomonas reinhardtii* share features with both mitochondrial and higher plant chloroplast presequences. *FEBS Lett* 260(2):165–168.

4. Emanuelsson O, Nielsen H, von Heijne G (1999) ChloroP, a neural network-based method for predicting chloroplast transit peptides and their cleavage sites. *Protein Science* 8(5):978–984.

5. Miura K, et al. (2004) Expression profiling-based identification of CO_2-responsive genes regulated by CCM1 controlling a carbon-concentrating mechanism in *Chlamydomonas. Plant Physiol* 135(3):1595–1607.

6. Moroney JV et al. (2011) The carbonic anhydrase isoforms of *Chlamydomonas reinhardtii*: intracellular location, expression, and physiological roles. *Photosynth Res* 109(1–3):133–149.

7. Wang Y, Spalding MH (2006) An inorganic carbon transport system responsible for acclimation specific to air levels of CO_2 in *Chlamydomonas reinhardtii. Proc Natl Acad Sci USA* 103(26):10110–10115.

8. Duanmu D, Wang Y, Spalding MH (2009) Thylakoid lumen carbonic anhydrase (CAH3) mutation suppresses air-Dier phenotype of *LCIB* mutant in *Chlamydomonas reinhardtii. Plant Physiol* 149(2):929–937.

9. Yamano T, et al. (2010) Light and low-CO_2-dependent LCIB-LCIC complex localization in the chloroplast supports the carbon-concentrating mechanism in *Chlamydomonas reinhardtii. Plant Cell Physiol* 51(9):1453–1468.

10. Wang Y, Spalding MH (2014) Acclimation to very low CO_2: contribution of limiting CO_2 inducible proteins, LCIB and LCIA, to inorganic carbon uptake in *Chlamydomonas reinhardtii. Plant Physiol* 166(4):2040–2050.

11. Blanco-Rivero A, Shutova T, Román MJ, Villarejo A, Martinez F (2012) Phosphorylation controls the localization and activation of the lumenal carbonic

anhydrase in *Chlamydomonas reinhardtii*. *PLoS One* 7(111):e49063.

SI Materials and Methods

Generation of Antibodies

Anti-LCIA, anti-HLA3, and anti-CCP1 antibodies were generated against synthetic peptides containing sequences with the 12 amino acids found at the C-terminus of LCIA (Cys-GSLGKSAKPATA), the 18 amino acids at the C-terminus of HLA3 (Cys-RKMAEDFWSTRSAQGRNQ), and the 13 amino acids at the C-terminus of CCP1 (Cys-VEGTRQGIKWYEE), respectively. Rabbits were injected with keyhole limpet hemocyanin-coupled to each synthetic peptide for the production of anti-LCIA polyclonal antibody (Hayashi Kasei, Osaka, Japan), anti-CCP1 polyclonal antibody (Hokkaido System Science, Hokkaido, Japan), and anti-HLA3 polyclonal antibody (Sigma-Aldrich, St. Louis, MO, USA), respectively. The anti-LCIA and anti-HLA3 antibodies were affinity purified.

Immunoblot Analyses

Total cell protein corresponding to 20 μg of chlorophyll was suspended in 200 μL of phosphate-buffered saline (PBS) with Complete protease inhibitor EDTA-free cocktail tablet (Roche, Mannheim, Germany) and sonicated with 30×2 s pulses using a sonicator (product number UR-21P from TOMY, Tokyo, Japan). Then, 200 μL of sodium dodecylsulfate (SDS) gel-loading buffer containing 50 mM Tris-HCl (pH 8.0), 25% glycerol (v/v), 2% SDS (w/v), and 0.1 M dithiothreitol was added to the solution, and the total cell protein was solubilized by incubation at 37°C for 20 min. Incubated samples were subsequently centrifuged at 14,000 g for 3 min, and 20 μL of each supernatant was subjected to 5–20% gradient gel SDS-PAGE (ATTO, Tokyo, Japan). For detecting H$^+$-ATPase, total cell protein corresponding to 2 μg of chlorophyll was directly suspended in 10 μL of SDS gel-loading buffer and incubated at 70°C for 10 min. Incubated samples were subsequently centrifuged at 21,500 g for 3 min and all of the supernatant was subjected to SDS-PAGE. In the case of protein immunoblot analysis for cell fractionation experiments, samples containing 10 μg of protein were homogenized in buffer containing 0.33 M sucrose, 50 mM MOPS-KOH (pH 7.0), 4 mM MgSO$_4$, and a Complete protease inhibitor EDTA-free cocktail tablet, mixed with 2×SDS gel-loading buffer to a volume of 20 μL, and then subjected to 5–20% gradient gel SDS-PAGE. After electrophoresis, proteins were electrophoretically

7

transferred to polyvinylidene difluoride (PVDF) membranes (Bio-Rad, Hercules, CA, USA) for 1 h. Membranes were blocked with 5% (w/v) non-fat skim milk (Wako, Osaka, Japan) in PBS for 1 h at room temperature. Blocked membranes were washed for 5 min with PBS containing 0.1% (v/v) Tween-20 (PBS-T; Santa Cruz Biotech, Dallas, TX, USA) and treated with the following antibodies in PBS-T for 1 h at room temperature: rabbit anti-LCIA antibody (1:5,000 dilution); rabbit anti-HLA3 antibody (1:1,000 or 1:2000 dilution); rabbit anti-LCI1 antibody (1:1,000 or 1:2000 dilution); rabbit anti-CCP1 antibody (1:2,500 dilution); rabbit anti-Histone H3 antibody (1:10,000 dilution; product number ab1791 from Abcam, Cambridge, MA, USA); or rabbit anti-H^+-ATPase antibody (1:2,500 dilution; product number AS07 260 from Agrisera, Vännäs, Sweden). Membranes were rinsed once and washed with PBS-T four times for 5 min each. A horseradish peroxidase (HRP)-conjugated goat anti-rabbit IgG antibody (1:10,000 dilution; GE Healthcare, Milwaukee, WI, USA) was used as a secondary antibody for 1 h at room temperature. Membranes were washed as described above, and immunologically positive signals were visualized using Luminata Crescendo Western HPR substrate (Millipore, Billerica, MA, USA) and detected using an ImageQuant LAS 4000 (Fuji Film, Tokyo, Japan). MagicMark XP Western Protein Standard (Life Technologies, Carlsbad, CA, USA) was used as a size marker.

Indirect Immunofluorescence Assay for LCIA and HLA3

Indirect immunofluorescence assays were done essentially as described previously (1). Briefly, *C. reinhardtii* cells suspended in PBS-T were affixed to poly-L-lysine-treated glass slides (Poly-Prep Slides, Sigma-Aldrich). Cells were fixed with 4% (w/v) formaldehyde in PBS, treated with 100% ice-cold methanol, and then rehydrated in PBS. Cells were blocked with 5% (w/v) bovine serum albumin in PBS. The slides with fixed cells were incubated for 1 h with affinity-purified anti-LCIA (1:100 dilution) and anti-HLA3 (1:200) antibodies, and then washed with PBS-T. Cells were incubated with Alexa Fluor 488 goat anti-rabbit IgG (1:500 dilution; Life Technologies), and washed as above. A series of digital optical sections of the fixed samples were obtained using an AF6000 fluorescence microscope (Leica, Wetzlar, Germany) with a specific filter set (excitation BP 480/40 and emission BP 527/30) or using confocal fluorescence microscopy TCS SP8 (Leica) with a 488 nm laser line.

Isolation of Chloroplast Envelope and Plasma Membrane Fractions

Intact chloroplasts were isolated from 12 L of strain CC-400 cells acclimated to very-low-CO_2 (VLC) conditions in accordance with a previous report (2). Isolated intact chloroplasts were collected by centrifugation at 680 g for 3 min and resuspended gently in 0.6 M sucrose buffer containing 10 mM Tris-NaOH (pH 8.0), 1 mM EDTA-NaOH (pH 8.0), and a Complete protease inhibitor EDTA-free cocktail tablet. After four freeze/thaw cycles, the suspension was homogenized and the molarity of sucrose was adjusted to 1.3 M by addition of 1.8 M sucrose buffer. This suspension was gently overlaid with 15 mL of 1.2 M and 10 mL of 0.3 M sucrose buffers, respectively, and centrifuged at 113,000 g overnight. The chloroplast envelopes (CE) were isolated as a yellow band at the interface of the 0.3 M and 1.2 M sucrose layers, diluted with buffer containing 10 mM Tris-NaOH (pH 8.0) and 1 mM EDTA-NaOH (pH 8.0), and pelleted by centrifugation at 113,000 g for 1 h. The pellet was resuspended in buffer containing 0.33 M sucrose, 50 mM MOPS-KOH (pH 7.0), 4 mM $MgSO_4$, and a Complete protease inhibitor EDTA-free cocktail tablet (Roche).

The procedure for the isolation of the plasma membranes (PM) fraction was adopted from a previous report (3) except that the breaking procedure for cells was performed using a BioNeb disruption system (AR BROWN, Tokyo, Japan) in accordance with the manufacturer's instructions.

For immunoblot analysis, protein samples from CE and PM fractions corresponding to 10 μg were separated by SDS-PAGE and then subjected to immunoblot analysis with antibodies against HLA3, the PM protein LCI1, the PM protein H^+-ATPase, LCIA, and the CE protein CCP1.

Isolation of the Thylakoid Membrane Fraction

For small-scale isolation of thylakoid membranes, 50 mL of *C. reinhardtii* cells were cultured in VLC conditions, collected by centrifugation at 600 g for 5 min at room temperature (RT), and resuspended in 5 mL of high-salt medium (HSM). This suspension was pelleted by centrifugation at 600 g for 5 min at RT, and the pellet was resuspended in 1 mL of HSM. This suspension was again pelleted by centrifugation at 600 g for 5 min at RT, washed once with Solution 1 (0.3 M sucrose, 1 mM $MgCl_2$, 25

mM HEPES-NaOH, pH 7.5), and resuspended in 100 µL of Solution 1. The cells were broken by vortexing with 800 mg of Zirconia/Silica beads (0.5 mm dia., BioSpec Products Inc., Bartlesville, OK, USA) for 5 min. The broken cells were recovered by washing the beads with 1.5 mL of Solution 1 and were then pelleted by centrifugation at 17,000 g for 20 min at 4°C. The pellets were washed with Solution 2 (0.3 M sucrose, 10 mM EDTA, 5 mM HEPES-NaOH, pH 7.5), suspended in 1.25 mL of Solution 3 (1.8 M sucrose, 10 mM EDTA, 25 mM HEPES-NaOH, pH 7.5), and then overlaid with 0.5 mL of Solution 4 (1.3 M sucrose, 10 mM EDTA, 5 mM HEPES-NaOH, pH 7.5) and 1.25 mL of Solution 5 (0.5 M sucrose, 10 mM EDTA, 5 mM HEPES-NaOH, pH 7.5). This discontinuous sucrose gradient was centrifuged at 208,000 g for 15 min at 4°C. The green band containing the thylakoid membranes present in the 1.3 M sucrose layer was collected, diluted with 3 volumes of Solution 6 (10 mM EDTA, 5 mM HEPES-NaOH, pH 7.5), centrifuged at 17,000 g for 30 min at 4°C, and then resuspended in Solution 6 at 0.8 mgChl^{-1} mL^{-1}.

Screening and Isolation of *HLA3* and *LCIA* Insertion Mutants

Insertion mutants were isolated essentially in accordance with a previous report (4). To generate an insertion mutant library, the *aphVIII* paromomycin-resistance gene (5), a 1,534-bp DNA fragment containing the paromomycin-resistance gene driven by a *HSP70A* (heat shock protein 70 A)-*RBCS2* tandem promoter (6), was amplified by PCR from plasmid pGenD-*aphVIII* (7) using PrimeSTAR GXL DNA Polymerase (Takara Bio, Shiga, Japan) by 30 cycles of denaturation for 10 s at 98°C, annealing for 15 s at 60°C, and extension for 2 min at 68°C with forward primer *aph*-F1 and reverse primer *aph*-R3. The PCR product was purified using a PCR purification kit (QIAGEN, Valencia, CA, USA), and the concentration was adjusted to 50 µg mL^{-1}. The *aphVIII* cassette was inserted into strain C9 as a marker gene using a high-efficiency electroporation method (8). Briefly, *C. reinhardtii* cells in early logarithmic phase were collected and transformed by electroporation using a 2-mm gap electroporation cuvette with a NEPA21 electroporator (Nepa Gene, Chiba, Japan). The transformants were incubated at 25°C for 24 h with gentle agitation and illumination at 1.5 µmol photons m^{-2} s^{-1} and then screened on Tris-acetate-phosphate (TAP) plates containing 10 µg mL^{-1} paromomycin. After isolation of individual colonies cultured in 96-well microtiter

plates containing 200 µL TAP liquid medium per well, 50 µL of each well was combined into one aliquot and cultured in 50 mL TAP medium. From this culture containing 96 transformants, genomic DNA was isolated and diluted to 50 µg mL^{-1}, designated as pools. Then, superpools that contained equal volumes of genomic DNA from 10 different pools were generated.

Screening for *LCIA* insertion mutants by PCR was performed using each DNA superpool as a template with marker gene primers RB1 and RB2 (4), and target gene primers *LCIA*-F1 to F3 and *LCIA*-R1 and R2. Screening for *HLA3* insertion mutants by PCR was performed using each DNA superpool as a template with newly designed marker gene primer RB-02 and target gene primers *HLA3*-F1 to F7 and *HLA3*-R1 to R7. PCR reactions were performed in a final volume of 10 µL and contained 0.3 pmoles of each primer, 0.2 mM of each dNTP, 0.5 U Ex-Taq DNA polymerase (Takara Bio), 1 µL 10 × Ex Taq DNA polymerase buffer, 0.4 M betain (Sigma-Aldrich), 100 ng of DNA template, and distilled water to make up the remainder of the 10 µL volume. Target gene primers were designed to be separated by approximately 1 kb from each primer. Consequently, screening of pools and individual transformants was performed to confirm the insertion mutant. The identified pool was sequenced using primer RB1, *LCIA*-F3, or *HLA3*-R5 to analyze the insertion site. Sequences of primers used in this study were shown in Table S4.

Ci-dependent Photosynthetic O$_2$-Evolving Activity

The inorganic carbon (Ci; CO$_2$ and HCO$_3^-$) affinity was evaluated by measuring the rate of dissolved Ci-dependent photosynthetic O$_2$ evolution. Cells were collected by centrifugation and then resuspended in Ci-depleted 50 mM HEPES-NaOH buffer (pH 7.8), 50 mM AMPSO-NaOH buffer (pH 9.0), and 50 mM MES-KOH buffer (pH 6.2) at 17.5 µg mL^{-1} chlorophyll. Photosynthetic O$_2$-evolving activity was measured using a Clark-type O$_2$ electrode (Hansatech Instruments, Norfolk, UK) in the presence of various concentrations of NaHCO$_3$ as described previously (9). Maximum O$_2$-evolving activity (V$_{max}$) was measured in the presence of 10 mM NaHCO$_3$.

Plasmid Construction and Transformation

The genomic sequence of *LCIA* was amplified by PCR with PrimeSTAR GXL (Takara

Bio) using genomic DNA extracted from strain C9 as a template with forward primer *LCIA*-BglII-F and reverse primer *LCIA*-EcoRI-R. The PCR product was cloned into expression vector pTY2b digesting with BglII and EcoRI (NCBI accession number AB447355). For the expression of *HLA3* and *LCI1*, a modified pTY2b expression vector harboring *aphVIII* was constructed and designated as pTY2b-aphVIII. For this, the region of the *ble* gene in the original pTY2b vector was replaced with the coding region of *aphVIII* amplified from plasmid pGenD-*aphVIII* (7) with forward primer aph-MluI-F and reverse primer *aph*-R. The *HLA3* and *LCI1* coding regions were amplified by PCR using PrimeSTAR GXL with forward primers *HLA3*-pTY2b-IF-F and *LCI1*-pTY2b-IF-F and reverse primers *HLA3*-pTY2b-IF-R and *LCI1*-pTY2b-IF-R, respectively, and then inserted into pTY2b-aphVIII using an InFusion reaction (Takara Bio). Transformation of the expression plasmid into *C. reinhardtii* cells was performed using a high-efficiency electroporation method (8) and screened on TAP plates containing 10 μg mL^{-1} Zeocin™ or 10 μg mL^{-1} paromomycin. Sequences of primers used in this study were shown in Table S4.

Intercellular Concentration of Dissolved Ci

The intercellular concentration of dissolved Ci was measured by the silicone oil centrifugation method as described previously (10). Cells were collected by centrifugation at 600 *g*, suspended at a cell density of approximately 25 μg mL^{-1} chlorophyll in Ci-depleted 50 mM HEPES-NaOH buffer (pH 7.8) or 50 mM AMPSO-NaOH buffer (pH 9.0), and 1.2 mL of the cell suspension was aerated with N$_2$ gas for 15 min in an O$_2$ electrode. First, a 60 μL silicone oil layer (SH550:SH556 = 4:7 [v/v]) was overlaid on a 20 μL layer of the termination solution containing 1 M glycine-NaOH, pH 10.0, and 0.75% SDS (w/v). Then, 300 μL of the cell suspension was further overlaid on the silicone oil layer. Ci uptake was initiated by the addition of 10 μL of 100 μM-NaH^{14}CO$_3$, which was immediately followed by 80, 160, or 240 s of illumination with an actinic light source of 300 μmol photons m^{-2} s^{-1}, and the reaction was terminated by centrifugation. After centrifugation, the labeled cells were immediately frozen using liquid nitrogen and then suspended in 400 μL of 0.1 N NaOH. The alkaline cell suspension was divided into two 160 μL aliquots. One was directly subjected to liquid scintillation counting, which was described as total Ci uptake. The

other aliquot was added to 200 μL of 0.5 N HCl, desiccated to liberate ^{14}C except for fixed $^{14}CO_2$, suspended in 200 μL of water, and then subjected to liquid scintillation counting to analyze the ^{14}C level, which was described as CO_2 fixation. Ci accumulation was calculated as the difference between the total Ci uptake and CO_2 fixation. Each value was corrected by estimating the cell volume as sorbitol impermeable space (SIS) using $[^{14}C]$ sorbitol and ^3H_2O as described previously (11).

Blue Native-PAGE

Total cell protein corresponding to 200 μg of chlorophyll was suspended in 200 μL of PBS with a Complete protease inhibitor EDTA-free cocktail tablet and sonicated with 30×2 s pulses. For the cross-linking experiment, 4% formaldehyde was added to the total protein solution and incubated on ice for 15 min before sonication. The crude extract was diluted in buffer containing 0.5% Coomassie Brilliant Blue (CBB)-G250 (Nacalai Tesque, Kyoto, Japan), 50 mM 6-aminocapronic acid, 10 mM Bis-Tris/HCl (pH 7.0), 1 mM phenylmethylsulfonyl fluoride (PMSF), 10% glycerol, and 0.25–1% n-dodecyl β-D-maltoside (DDM; Dojindo, Kumamoto, Japan), and incubated on ice for 20 min. Incubated samples were subsequently centrifuged at 21,500 g for 3 min, and the supernatant was loaded onto a NativePAGE™ Novex® 4-16 Bis-Tris gel (Invitrogen) in accordance with the manufacturer's instructions. NativeMark Unstained Protein Standard (Invitrogen) was used as a size marker. After electrophoresis, the gel was immersed in buffer containing 20 mM Tris, 150 mM glycine, and 0.1% SDS for 10 min to denature the protein, and then transferred to a PVDF membrane. The membrane was incubated in 8% acetic acid to fix the proteins and then reacted with an antibody as described above.

Quantitative (q) Real-Time (RT) PCR

qRT-PCR was performed using SYBR Premix Ex Taq GC (Takara Bio) and a LightCycler 480 Instrument (Roche) as described previously (12). The amplification conditions were as follows: 5 min denaturation at 95°C; 40 cycles at 95°C for 10 s, at 55°C for 30 s and at 68°C for 1 min. Melting curves for each PCR product were determined by measuring the decrease in fluorescence with increasing temperature from 60°C to 95°C. *CBLP* encoding *Chlamydomonas* beta subunit-like polypeptide (13) was

used as an internal control. The primers used for qRT-PCR are listed in Table S4.

1. Yamano T, et al. (2010) Light and low-CO_2-dependent LCIB-LCIC complex localization in the chloroplast supports the carbon-concentrating mechanism in *Chlamydomonas reinhardtii*. *Plant Cell Physiol* 51(9):1453–1468.

2. Mason CB, Bricker TM, Moroney JV (2006) A rapid method for chloroplast isolation from the green alga *Chlamydomonas reinhardtii*. *Nat Protoc* 1(5):2227–2230.

3. Norling B, Nurani G, Franzen LG (1996) Characterization of the H^+-ATPase in plasma membranes isolated from the green alga *Chlamydomonas reinhardtii*. *Physiol Plant* 97(3):445–453.

4. Gonzalez-Ballester D, et al. (2011) Reverse genetics in Chlamydomonas: a platform for isolating insertional mutants. *Plant Methods* 7:24.

5. Sizova I, Fuhrmann M, Hegemann P (2001) A *Streptomyces rimosus aphVIII* gene coding for a new type phosphotransferase provides stable antibiotic resistance to *Chlamydomonas reinhardtii*. *Gene* 277(1–2):221–229.

6. Lodha M, Schulz-Raffelt M, Schroda M (2008) A new assay for promoter analysis in *Chlamydomonas* reveals roles for heat shock elements and the TATA box in *HSP70A* promoter-mediated activation of transgene expression. *Eukaryot Cell* 7(1):172–176.

7. Nakazawa Y, Hiraki M, Kamiya R, Hirono M (2007) SAS-6 is a cartwheel protein that establishes the 9-fold symmetry of the centriole. *Curr Biol* 17(24):2169–2174.

8. Yamano T, Iguchi H, Fukuzawa H (2013) Rapid transformation of *Chlamydomonas reinhardtii* without cell-wall removal. *J Biosci Bioeng* 115(6):691–694.

9. Yamano T, Miura K, Fukuzawa H (2008) Expression analysis of genes associated with the induction of the carbon-concentrating mechanism in *Chlamydomonas reinhardtii*. *Plant Physiol* 147(1):340–354.

10. Ohnishi N, et al. (2010) Expression of a low CO_2-inducible protein, LCI1, increases inorganic carbon uptake in the green alga *Chlamydomonas reinhardtii*. *Plant Cell* 22(9):3105–3117.

11. Heldt HW (1980) Measurement of metabolite movement across the envelope and of the pH in the stroma and the thylakoid space in intact chloroplasts. *Methods*

Enzymol 69:604–613.

12. Wang L, Yamano T, Kajikawa M, Hirono M, Fukuzawa H (2014) Isolation and characterization of novel high-CO_2-requiring mutants of *Chlamydomonas reinhardtii*. *Photosynth Res* 121(2-3):175–184.

13. Schloss JA (1990) A Chlamydomonas gene encodes a G protein beta subunit-like polypeptide. *Mol Gen Genet* 221(3):443-452.

Supporting Figure Legends

Fig. S1. Accumulation and subcellular localization of HLA3 and LCIA. (*A*) Accumulation of HLA3 and LCIA in WT and C16 (CCM1-deficient regulatory mutant) cells was analyzed by immunoblot analysis. Cells were grown in continuous high CO_2 (HC) or very low CO_2 (VLC) conditions for 12 h. kDa, kilodalton. (*B*) Reduction in HLA3 and H^+-ATPase aggregation. Aggregation of HLA3 (*Upper*) and H^+-ATPase (*Lower*) in the plasma membrane (PM) fraction was significantly reduced by serial dilution of the sample. Total cell proteins were isolated from strain CC-400 grown in HC or VLC conditions. PM fractions were isolated from strain CC-400 grown in VLC conditions. Aliquots of total cell protein correspond to 2 μg of chlorophyll and PM fractions corresponding to 10 μg of protein were loaded in the lanes designated as ×1 and the same amounts of protein was serially diluted to 8, 6, 5, 4, 2, or 1 μg of protein. Solubilized proteins were separated using 7.5% SDS-PAGE gels. (*C*) Immunoblot analysis for HLA3 and LCIA in isolated thylakoid membrane fractions. Total cell proteins were isolated from WT cells grown in HC or VLC conditions. Thylakoid membrane fractions were isolated from WT cells grown in VLC conditions. Samples corresponding to 2 μg of chlorophyll were separated by SDS-PAGE and then subjected to immunoblot analysis with antibodies against HLA3, LCIA, and the thylakoid membrane protein D1. (*D*) Subcellular localization of LCIA and HLA3 in LCIA-overexpressing strain Aox-1 and HLA3-overexpressing strain Hox-1 were analyzed by an indirect immunofluorescence method using affinity-purified antibodies against LCIA and HLA3, respectively. Aox-1 and Hox-1 were grown in HC-NO_3^- conditions. DIC, differential interference contrast; scale bars, 5 μm.

Fig. S2. Isolation and characterization of *HLA3* and/or *LCIA* insertion mutants. (*A*) Schematic representation of *aphVIII* cassettes inserted into the genomic sequence of *HLA3* in the *HLA3*-insertion mutant Hin-1, and the positions of primers. Tall boxes denote exons; filled boxes indicate protein coding regions; open boxes show 5'- and 3'-UTRs; gray boxes with arrows indicate *aphVIII* cassettes with their directions; arrowheads indicate the position of each primer. (*B*) Genomic PCR using WT, and Hin-1 template DNA with the primers depicted in (*A*). Primer sets used are indicated above the strain names. kb, kilobase pair. (*C*) Accumulation of HLA3, LCIA, LCI1, and

LCIB in WT, Hin-1, and the complemented strain Hin-1C. Cells were grown in very low CO_2 (VLC) conditions for 12 h. Histone H3 was used as a loading control. (*D*) Schematic representation of *aphVIII* cassettes inserted into the genomic sequence of *LCIA* in the *LCIA*-insertion mutants Ain-1 and Ain-2, and the positions of primers. Tall boxes denote exons; filled boxes indicate protein coding regions; open boxes show 5'- and 3'-UTRs; gray boxes with arrows indicate *aphVIII* cassettes with their directions; arrowheads indicate the position of each primer. (*E*) Genomic PCR using WT, Ain-1, and Ain-2 template DNA with the primers depicted in (*D*). Primer sets used are indicated above the strain names. kb, kilobase pair. (*F*) Insertion sites of the *aphVIII* PCR cassette in Ain-1, Ain-2, and *lab1*, a previously isolated *LCIA*-insertion mutant (1). Transmembrane regions were predicted using the SOSUI program (http://harrier.nagahama-i-bio.ac.jp/sosui/). The chloroplast transit peptide predicted using the ChloroP program (http://www.cbs.dtu.dk/services/ChloroP/) was cleaved. Red circles indicate amino acid residues conserved in FocA homologs that form the pore; yellow circles indicate epitope sequences for constructing the anti-LCIA antibody; boxes show predicted transmembrane regions; arrowheads indicate the insertion sites of the *aphVIII* PCR cassette in Ain-1, Ain-2, and *lab1*. (*G*) Southern blot analysis of WT, Ain-1, and Ain-2. Genomic DNA was extracted from each strain and digested with *Pst*I. In total, 10 μg of DNA was loaded and probed with a ^{32}P-labeled *aphVIII* PCR cassette. The *aphVIII* PCR cassette (0.02 ng) was used as a positive control. (*H*) Genotyping of WT, CC-1690, Ain-2, and Ain-2×CC-1690 progenies (B1–B8). Primer sets used are indicated on the right. Mating type (mt) of the progenies were determined using primer sets annealed to *MID* for mt$^-$ and *FUS* for mt$^+$. Progenies with labels in red (B4, B6, B7, and B8) harbored *aphVIII* insertion into *LCIA* loci. (*I*) Inorganic carbon (Ci) affinity of WT, CC-1690, and Ain-2×CC-1690 progenies. Photosynthetic O_2-evolving activity of these strains was measured in different external Ci concentrations at pH 9.0 and the respective $K_{0.5}$ (Ci) values, the Ci concentration required for half maximum O_2-evolving activity (V_{max}), were calculated. All cells were grown in VLC conditions for 12 h. Gray-colored bars indicated the decreased Ci affinity compared with WT and CC-1690 cells. (*J*) Strategy to obtain *LCIA*/*HLA3* double-insertion mutants by genetic crossing. (*K*) Genotyping of B4×Hin-1 progenies (D1–D7). Primer sets used are indicated on the right. Progenies with labels in red (D1 and D4) harbored the *aphVIII* insertions into

17

both the *LCIA* and *HLA3* loci. *CBLP* was used as a loading control. (*L*) Growth curves of WT, Hin-1, Ain-1, Ain-2, and AHin-2 cells at pH 8.4. Each strain was grown in Tris-acetate-phosphate (TAP) medium and then diluted with high-salt medium (HSM) supplemented with 20 mM MOPS (pH 7.0) in VLC conditions for over 12 h. Subsequently, cells were collected by centrifugation, resuspended in HSM supplemented with 20 mM Tris-NaOH (pH8.4), and diluted to an optical density at 730 nm (OD_{730}) of 0.015. Cells were grown with air containing 0.04% CO_2 and OD_{730} was measured at the indicated time points.

Fig. S3. Isolation of LCIA- and/or HLA3-overexpressing strains. (*A*) A schematic illustration of the chimeric constructs for the exogenous expression of *LCIA*, *HLA3*, and *LCI1*. Tandemly duplicated enhancer elements of *NIA1* encoding nitrate reductase (2) and the minimal promoter of TUB2 encoding β2-tublin were fused to the 5'-UTR and genomic sequence of *LCIA*, *HLA3*, or *LCI1* followed by the 3'-UTR of *RBCS2* coding for the small subunit of Rubisco. The genes shown as filled boxes are the *ble* gene (3) and the *aphVIII* gene (4), which permit growth in the presence of Zeocin™ and paromomycin, respectively. (*B* and *C*) Accumulation of LCIA in WT and LCIA-overexpressing strains Aox-1 and Aox-2 (*B*) and that of HLA3 in WT and HLA3-overexpressing strains Hox-1 and Hox-2 (*C*). To compare the accumulation levels of LCIA and HLA3 with that in WT, aliquots of total cell protein corresponding to 2 μg of chlorophyll were loaded in the lane designated as ×1, and the same amount of protein was serially diluted 2 to 128 times and loaded in the lanes designated ×2, ×4, ×8, ×16, ×32, ×64, and ×128. Solubilized proteins were separated in a 15% SDS-PAGE gel for detecting LCIA and in a 6% SDS-PAGE gel for HLA3. (*D*) Accumulation of LCIA and HLA3 in WT and LCIA/HLA3-overexpressing strains AHox-1 and AHox-2. (*E*) Accumulation of LCIA and HLA3 in WT and LCIA/HLA3-overexpressing strain AHox-3. (*F*) Accumulation of LCIA and LCI1 in WT and LCIA/LCI1-overexpressing strains A1ox-1 and A1ox-2.

Fig. S4. Molecular sizes of LCIA and HLA3 in non-denaturing conditions and the effect of LCIA on *HLA3* mRNA accumulation. (*A*) Molecular masses of LCIA and HLA3 in WT cells in non-denaturing conditions. Total proteins were solubilized using

n-dodecyl β-D-maltoside (DDM) at difference concentrations (0.25%, 0.5%, 1.0%, or 2.0%) and loaded on a Blue Native-PAGE gel. Molecular masses of LCIA and HLA3 were estimated by comparison with the migration of size markers as indicated. Native Mark (Invitrogen) was loaded as a size marker. (*B*) Molecular masses of LCIA and HLA3 in WT, Ain-2, and Hin-1 cells treated with formaldehyde (FA) cross-linker in non-denaturing conditions. Total proteins were cross-linked with 4% FA, solubilized using DDM, and loaded onto blue-native PAGE gels. (*C*) Molecular masses of LCIA and HLA3 in high-CO_2 grown Aox-1, Hox-1, and AHox-1 strains in non-denaturing conditions. Total proteins were solubilized using 1.0% DDM and separated by blue-native PAGE. (*D*) Quantitative real-time PCR analyses of *LCIB* and *LCI1* in WT, Ain-1, Ain-2, Ain-1C, Ain-2C, Hin-1, and Hin-1C. These cells were grown in very low CO_2 conditions for 4 h. Expression of each gene was normalized to *CBLP*. Data in all experiments indicate mean value ± SD from three biological replicates.

1. Wang Y, Spalding MH (2014) Acclimation to very low CO_2: contribution of limiting CO_2 inducible proteins, LCIB and LCIA, to inorganic carbon uptake in *Chlamydomonas reinhardtii*. *Plant Physiol* 166(4):2040–2050.

2. Loppes R, Radoux M (2002) Two short regions of the promoter are essential for activation and repression of the nitrate reductase gene in *Chlamydomonas reinhardtii*. *Mol Genet Genomics* 268(1):42–48.

3. Lumbreras V, Stevens DR, Purton S (1998) Efficient foreign gene expression in *Chlamydomonas reinhardtii* mediated by an endogenous intron. *Plant J* 14(4):441–447.

4. Sizova I, Fuhrmann M, Hegemann P (2001) A *Streptomyces rimosus aphVIII* gene coding for a new type phosphotransferase provides stable antibiotic resistance to *Chlamydomonas reinhardtii*. *Gene* 277(1–2):221–229.

A

	5% (HC)	1	2	4	6	12	[h]

0.04%

HLA3 (133 kDa)

LCIA (27 kDa)

LCI1

Histone H3

Ci: 5,180 28.2 13.7 13.0 8.7 8.2 [μM]
CO₂: 1,160 6.3 3.1 2.9 1.9 1.8 [μM]

B

DIC   anti-HLA3

DIC   anti-LCIA

C

Total protein		PM	CE
HC	VLC	VLC	VLC

HLA3

LCI1

H⁺-ATPase

Total protein		PM	CE
HC	VLC	VLC	VLC

*
*
LCIA
*

CCP1

A WT | Ain-1 | Ain-1C | Ain-2 | Ain-2C

- LCIA
- HLA3
- LCI1
- LCIB
- Histone H3

B

pH 6.2

$K_{0.5}(Ci)$ [μM]

- WT
- Ain-1
- Ain-1C
- Ain-2
- Ain-2C

6h 12h

pH 7.8

6h 12h

C

pH 9.0

$K_{0.5}(Ci)$ [μM]

- WT
- Ain-1
- Ain-1C
- Ain-2
- Ain-2C

HC 1h 2h 4h 6h 12h

D WT | AHin-1 | AHin-2

- LCIA
- HLA3
- Histone H3

E

$K_{0.5}(Ci)$ [μM]

pH 6.2

6h 12h

pH 7.8

6h 12h

pH 9.0

- WT
- AHin-2

HC 6h 12h

F

Ci accumulation [mM]

- WT VLC
- WT HC
- AHin-2 VLC

0 80 160 240
Illumination time [s]

CO_2 fixation [nmol μL SIS^{-1}]

- WT VLC
- WT HC
- AHin-2 VLC

0 80 160 240
Illumination time [s]

A

LCIA
(240 kDa)

(kDa)
1048
720
480
242
146

HLA3
(580 kDa)

WT   Ain-2   Hin-1   WT   Ain-2   Hin-1

B

Relative expression

1.5

1.0

0.5

0

1.5

1.0

0.5

0

*   *   *

*   *

WT   Ain-1 Ain-1C Ain-2 Ain-2C Hin-1 Hin-1C

Fig. S1

A

WT   C16

HC VLC   HC VLC   (kDa)

HLA3
(133 kDa)

LCIA
(27 kDa)

- 220
- 120
- 100

- 40
- 30
- 20

B

Total
protein   PM isolated from VLC conditions

HC VLC   10   8   6   5   4   2   1   (μg protein)

Aggregated
HLA3

HLA3

Total
protein   PM isolated from VLC conditions

HC VLC   10   8   6   5   4   2   1   (μg protein)

Aggregated
H⁺-ATPase

H⁺-ATPase

C

Total
protein   Thylakoid

HC VLC   VLC

HLA3

D1

Total
protein   Thylakoid

HC VLC   VLC

LCIA

D1

D

DIC   anti-LCIA

DIC   anti-HLA3

Fig. S2

A

Hin-1
(Δ3-bp in *HLA3*)

RB1

F5

HLA3

R5

B

| R5/RB1 | F5/R5 |
| WT Hin-1 | WT Hin-1 |

(kb)   (kb)

3.0

1.5

0.8

C

WT Hin-1 Hin-1C

HLA3

LCIA

LCI1

LCIB

Histone H3

D

Ain-1
(3-bp insertion in *LCIA*)

RB1

F2   F3

LCIA

R1   R2

RB1

Ain-2
(Δ28-bp in *LCIA*)

E

| F3/RB1 | F3/R2 |
| WT Ain-1 Ain-2 | WT Ain-1 Ain-2 |

(kb)   (kb)

2.8

1.0   0.8

0.2

F

NH₂

COOH

Ain-2

Ain-1

lab1
(Wang and Spalding 2014)

G

Ain-1 Ain-2 WT *aphVIII*

(kb)   (kb)

12

6.0
5.0   4.7
4.0   4.1
                              3.35
3.0

1.65

1.0

H

Ain-2 × CC-1690

WT CC-1690 Ain-2 B1 B2 B3 **B4** B5 **B6** **B7** **B8**

F3/R2

F2/R1

MID
(*mt⁻* marker)

FUS
(*mt⁺* marker)

I

$K_{0.5}$ (Ci) [μM]

800

600

400

200

WT CC-1690 Ain-2 B1 B2 B3 B4 B5 B6 B7 B8

J

Ain-2 (mt⁻) × CC-1690 (mt⁺)

Progenies (B1–B8)

B4 (mt⁺) × Hin-1 (mt⁻)

Progenies (D1–D7)

K

Ain-2 progeny B4 × Hin-1

D1 D2 D3 **D4** D5 D6 D7

LCIA (F3/R2)

HLA3 (F5/R5)

CBLP

L

Optical density at 730 nm

1.6

1.4

1.2

1.0

0.8

0.6

0.4

0.2

0

WT

Hin-1

Ain-2

Ain-1

AHin-2

0 12 24 36 48 60

Time [h]

Fig. S3

Fig. S4

A

DDM
0.25 0.5 1.0 2.0 (%)

DDM
0.25 0.5 1.0 2.0 (%)   (kDa)

1048
720
480
242
146

LCIA
(240 kDa)

HLA3
(580 kDa)

B

4% FA
WT Ain-2 Hin-1

4% FA
WT Ain-2 Hin-1   (kDa)

1048
720
480
242
146

LCIA
(240 kDa)

HLA3
(580 kDa)

C

Aox-1 AHox-1

Hox-1 AHox-1   (kDa)

1048
720
480
242
146

LCIA
(240 kDa)

HLA3
(580 kDa)

D

Relative expression

LCIB

1.5
1.0
0.5
0

LCI1

1.5
1.0
0.5
0

WT Ain-1 Ain-1C Ain-2 Ain-2C Hin-1 Hin-1C

Table S1. Photosynthetic parameters of WT and transformant cells at pH 6.2

Strain name	Growth conditions	V_{max} of O_2-evolving activity [μmol O_2 mgChl^{-1} h^{-1}]	$K_{0.5}$ (Ci) [μM]
WT	VLC-NH$_4^+$ for 6 h	209 ± 11	27 ± 3
	VLC-NH$_4^+$ for 12 h	214 ± 9	26 ± 3
	HC-NO$_3^-$ for 12 h	272 ± 41	55 ± 4
Hin-1	VLC-NH$_4^+$ for 6 h	223 ± 19	25 ± 4
	VLC-NH$_4^+$ for 12 h	210 ± 9	27 ± 3
Ain-1	VLC-NH$_4^+$ for 6 h	201 ± 17	25 ± 2
	VLC-NH$_4^+$ for 12 h	213 ± 8	24 ± 3
Ain-1C	VLC-NH$_4^+$ for 6 h	212 ± 13	27 ± 3
	VLC-NH$_4^+$ for 12 h	207 ± 8	27 ± 3
Ain-2	VLC-NH$_4^+$ for 6 h	229 ± 17	26 ± 2
	VLC-NH$_4^+$ for 12 h	223 ± 12	24 ± 4
Ain-2C	VLC-NH$_4^+$ for 6 h	238 ± 19	27 ± 1
	VLC-NH$_4^+$ for 12 h	212 ± 14	27 ± 2
AHin-2	VLC-NH$_4^+$ for 6 h	221 ± 25	22 ± 5
	VLC-NH$_4^+$ for 12 h	236 ± 37	20 ± 7
Aox-1	HC-NO$_3^-$ for 12 h	266 ± 30	31 ± 5
Aox-2	HC-NO$_3^-$ for 12 h	279 ± 50	31 ± 9
Hox-1	HC-NO$_3^-$ for 12 h	223 ± 18	62 ± 5
Hox-2	HC-NO$_3^-$ for 12 h	219 ± 27	50 ± 9
AHox-1	HC-NO$_3^-$ for 12 h	221 ± 20	39 ± 5
AHox-2	HC-NO$_3^-$ for 12 h	232 ± 15	41 ± 12
AHox-3	HC-NO$_3^-$ for 12 h	218 ± 31	33 ± 4
A1ox-1	HC-NO$_3^-$ for 12 h	199 ± 29	30 ± 4
A1ox-2	HC-NO$_3^-$ for 12 h	208 ± 11	25 ± 9

The data are shown ± standard deviation, which were obtained from at least three independent experiments. HC, high-CO_2; $K_{0.5}$ (Ci), Ci concentration required for half V_{max}; VLC, very-low-CO_2; V_{max}, maximum O_2-evolving activity; WT, wild-type.
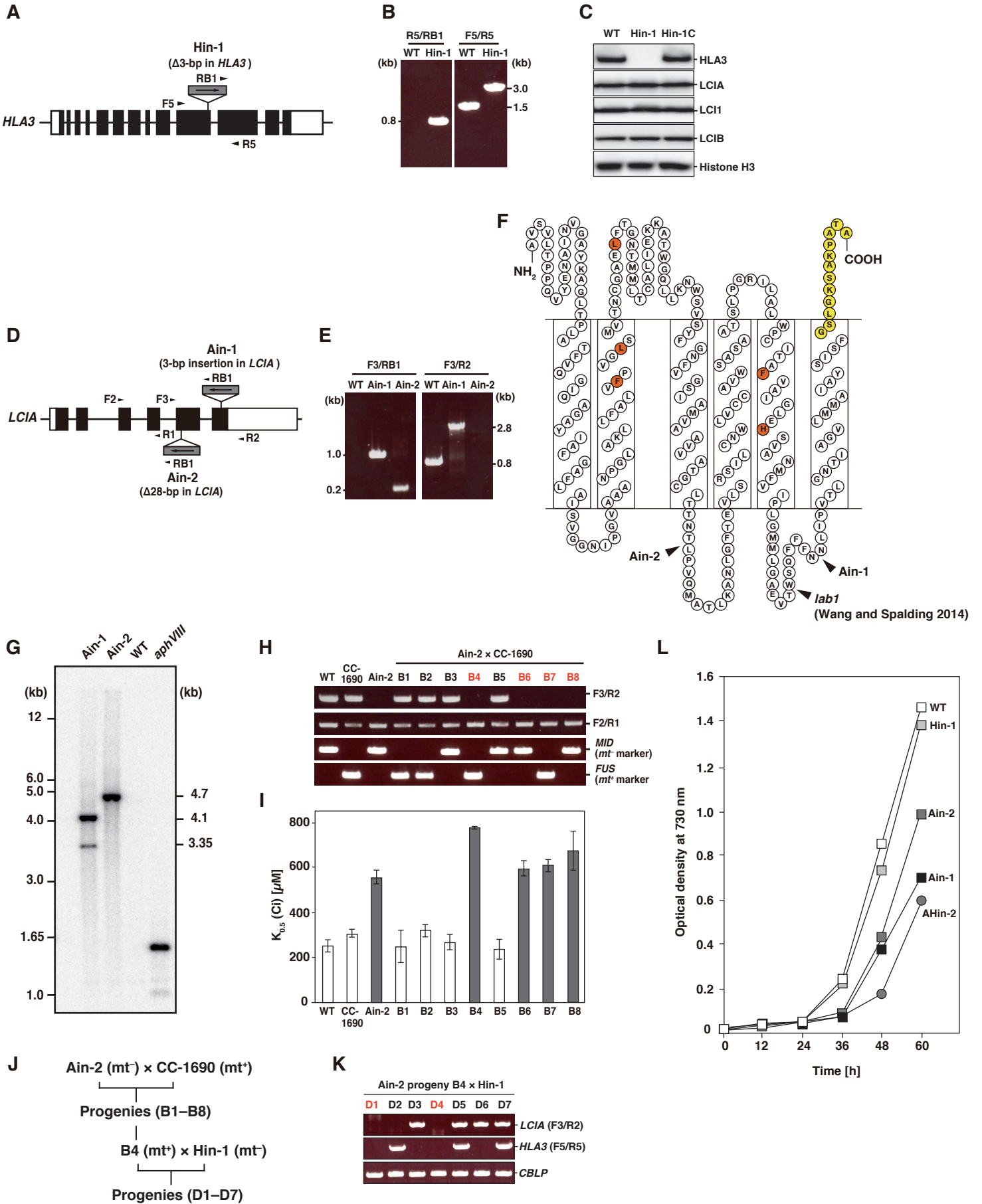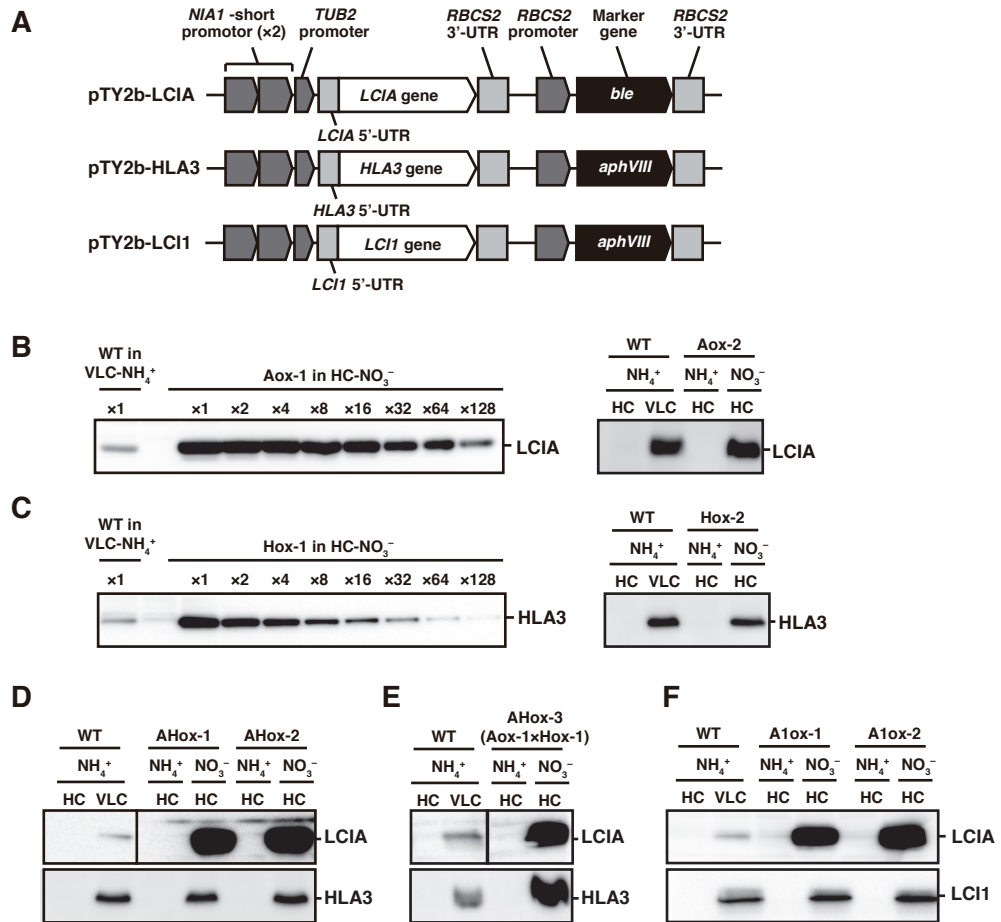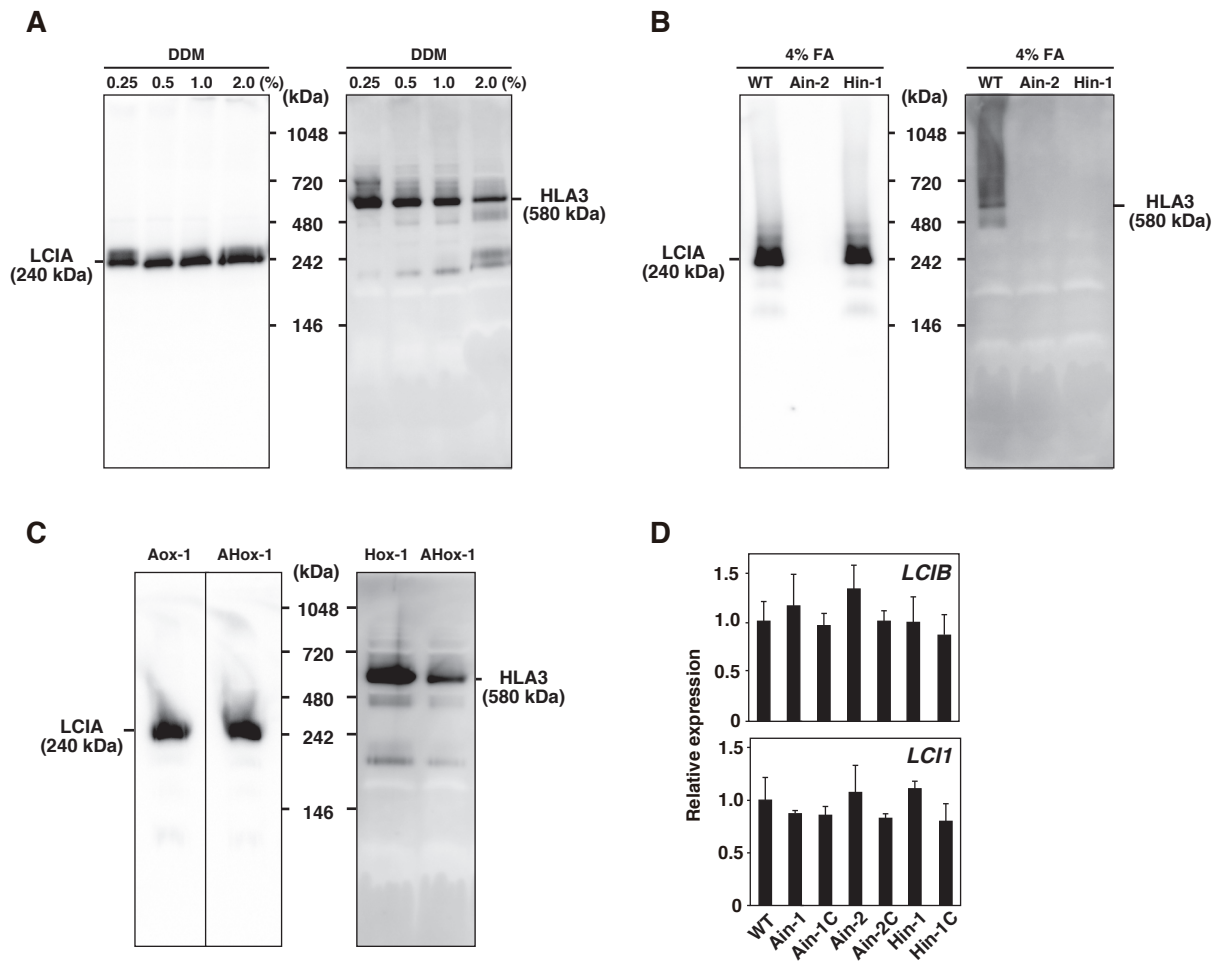
Table S2. Photosynthetic parameters of WT and transformant cells at pH 7.8

Strain name	Growth conditions	V_{max} of O_2-evolving activity [μmol O_2 mgChl^{-1} h^{-1}]	$K_{0.5}$ (Ci) [μM]
WT	VLC-NH_4^+ for 6 h	218 ± 13	40 ± 3
	VLC-NH_4^+ for 12 h	232 ± 36	33 ± 3
	HC-NH_4^+ for 12 h	211 ± 23	273 ± 31
	HC-NO_3^- for 12 h	199 ± 16	230 ± 27
Hin-1	VLC-NH_4^+ for 6 h	201 ± 21	48 ± 4
	VLC-NH_4^+ for 12 h	230 ± 32	42 ± 10
Ain-1	VLC-NH_4^+ for 6 h	213 ± 15	57 ± 2
	VLC-NH_4^+ for 12 h	231 ± 14	56 ± 3
Ain-1C	VLC-NH_4^+ for 6 h	201 ± 17	38 ± 2
	VLC-NH_4^+ for 12 h	220 ± 8	32 ± 2
Ain-2	VLC-NH_4^+ for 6 h	220 ± 17	57 ± 1
	VLC-NH_4^+ for 12 h	212 ± 9	57 ± 2
Ain-2C	VLC-NH_4^+ for 6 h	218 ± 10	37 ± 3
	VLC-NH_4^+ for 12 h	209 ± 19	29 ± 2
AHin-2	VLC-NH_4^+ for 6 h	202 ± 8	58 ± 2
	VLC-NH_4^+ for 12 h	208 ± 4	61 ± 10
Aox-1	HC-NO_3^- for 12 h	211 ± 24	211 ± 22
Aox-2	HC-NO_3^- for 12 h	197 ± 30	211 ± 27
Hox-1	HC-NO_3^- for 12 h	190 ± 29	208 ± 21
Hox-2	HC-NO_3^- for 12 h	211 ± 17	216 ± 11
AHox-1	HC-NH_4^+ for 12 h	212 ± 7	257 ± 28
	HC-NO_3^- for 12 h	230 ± 22	141 ± 20
AHox-2	HC-NH_4^+ for 12 h	217 ± 19	250 ± 30
	HC-NO_3^- for 12 h	227 ± 32	174 ± 20
AHox-3	HC-NH_4^+ for 12 h	231 ± 8	262 ± 29
	HC-NO_3^- for 12 h	224 ± 19	147 ± 19
A1ox-1	HC-NO_3^- for 12 h	226 ± 38	259 ± 8
A1ox-2	HC-NO_3^- for 12 h	254 ± 21	264 ± 29
A1ox-3	HC-NO_3^- for 12 h	221 ± 18	229 ± 39
A1ox-4	HC-NO_3^- for 12 h	219 ± 9	232 ± 18
A1ox-5	HC-NO_3^- for 12 h	232 ± 17	260 ± 15
A1ox-6	HC-NO_3^- for 12 h	212 ± 23	249 ± 21

The data are shown ± standard deviation, which were obtained from at least three independent experiments. HC, high-CO_2; $K_{0.5}$ (Ci), Ci concentration required for half V_{max}; VLC, very-low-CO_2; V_{max}, maximum O_2-evolving activity; WT, wild-type.

Table S3. Photosynthetic parameters of WT and transformant cells at pH 9.0

Strain name	Growth conditions	V_{max} of O_2-evolving activity [$\mu mol\ O_2\ mgChl^{-1}\ h^{-1}$]	$K_{0.5}$ (Ci) [μM]
WT	HC-NH_4^+	198 ± 31	2658 ± 120
	VLC-NH_4^+ for 1 h	201 ± 18	890 ± 88
	VLC-NH_4^+ for 2 h	221 ± 33	450 ± 70
	VLC-NH_4^+ for 4 h	203 ± 17	391 ± 90
	VLC-NH_4^+ for 6 h	215 ± 24	241 ± 87
	VLC-NH_4^+ for 12 h	222 ± 21	290 ± 50
	HC-NO_3^- for 12 h	212 ± 21	2650 ± 80
Hin-1	HC-NH_4^+	189 ± 21	2580 ± 89
	VLC-NH_4^+ for 1 h	180 ± 12	1472 ± 90
	VLC-NH_4^+ for 2 h	191 ± 23	981 ± 87
	VLC-NH_4^+ for 4 h	194 ± 11	790 ± 120
	VLC-NH_4^+ for 6 h	225 ± 47	691 ± 143
	VLC-NH_4^+ for 12 h	223 ± 16	405 ± 57
Hin-1C	HC-NH_4^+	202 ± 32	2820 ± 76
	VLC-NH_4^+ for 1 h	181 ± 9	1007 ± 45
	VLC-NH_4^+ for 2 h	191 ± 18	486 ± 67
	VLC-NH_4^+ for 4 h	212 ± 11	462 ± 34
	VLC-NH_4^+ for 6 h	251 ± 12	296 ± 78
	VLC-NH_4^+ for 12 h	244 ± 18	333 ± 89
Ain-1	HC-NH_4^+	230 ± 18	2592 ± 89
	VLC-NH_4^+ for 1 h	248 ± 22	1906 ± 89
	VLC-NH_4^+ for 2 h	285 ± 31	1221 ± 120
	VLC-NH_4^+ for 4 h	268 ± 18	1047 ± 78
	VLC-NH_4^+ for 6 h	267 ± 21	767 ± 70
	VLC-NH_4^+ for 12 h	243 ± 19	551 ± 65
Ain-1C	HC-NH_4^+	221 ± 23	2600 ± 65
	VLC-NH_4^+ for 1 h	238 ± 11	1034 ± 76
	VLC-NH_4^+ for 2 h	240 ± 17	502 ± 110
	VLC-NH_4^+ for 4 h	281 ± 31	420 ± 65
	VLC-NH_4^+ for 6 h	250 ± 11	278 ± 45
	VLC-NH_4^+ for 12 h	272 ± 29	285 ± 38
Ain-2	HC-NH_4^+	211 ± 13	2620 ± 78
	VLC-NH_4^+ for 1 h	208 ± 12	1833 ± 110
	VLC-NH_4^+ for 2 h	231 ± 8	1357 ± 90
	VLC-NH_4^+ for 4 h	241 ± 26	821 ± 76
	VLC-NH_4^+ for 6 h	232 ± 18	720 ± 56
	VLC-NH_4^+ for 12 h	233 ± 16	479 ± 64
Ain-2C	HC-NH_4^+	221 ± 15	2654 ± 82
	VLC-NH_4^+ for 1 h	228 ± 9	900 ± 131
	VLC-NH_4^+ for 2 h	239 ± 21	531 ± 56
	VLC-NH_4^+ for 4 h	212 ± 25	432 ± 91
	VLC-NH_4^+ for 6 h	212 ± 5	290 ± 31
	VLC-NH_4^+ for 12 h	224 ± 13	244 ± 39
AHin-2	HC-NH_4^+	221 ± 21	2620 ± 89
	VLC-NH_4^+ for 6 h	233 ± 12	898 ± 78
	VLC-NH_4^+ for 12 h	246 ± 42	901 ± 94

Continued Table S3.

Strain name	Growth conditions	V_{max} of O_2-evolving activity [μmol O_2 mgChl^{-1} h^{-1}]	$K_{0.5}$ (Ci) [μM]
Aox-1	HC-NO_3^- for 12 h	228 ± 11	2550 ± 72
Aox-2	HC-NO_3^- for 12 h	211 ± 15	2690 ± 120
Hox-1	HC-NO_3^- for 12 h	199 ± 25	2541 ± 121
Hox-2	HC-NO_3^- for 12 h	208 ± 13	2393 ± 94
AHox-1	HC-NO_3^- for 12 h	209 ± 17	1821 ± 201
AHox-2	HC-NO_3^- for 12 h	201 ± 19	1980 ± 198
AHox-3	HC-NO_3^- for 12 h	218 ± 21	1626 ± 49
A1ox-1	HC-NO_3^- for 12 h	210 ± 17	2670 ± 180
A1ox-2	HC-NO_3^- for 12 h	225 ± 12	2803 ± 82
A1ox-3	HC-NO_3^- for 12 h	221 ± 19	2789 ± 112
A1ox-4	HC-NO_3^- for 12 h	232 ± 21	2675 ± 78
A1ox-5	HC-NO_3^- for 12 h	209 ± 28	2901 ± 121
A1ox-6	HC-NO_3^- for 12 h	201 ± 17	2877 ± 88
CC-1690	VLC-NH_4^+ for 12 h	202 ± 6	300 ± 25
B1 (Progeny of Ain-2×CC-1690)	VLC-NH_4^+ for 12 h	218 ± 16	247 ± 74
B2	VLC-NH_4^+ for 12 h	229 ± 13	319 ± 25
B3	VLC-NH_4^+ for 12 h	259 ± 9	268 ± 31
B4	VLC-NH_4^+ for 12 h	244 ± 5	774 ± 9
B5	VLC-NH_4^+ for 12 h	239 ± 3	235 ± 43
B6	VLC-NH_4^+ for 12 h	243 ± 5	592 ± 42
B7	VLC-NH_4^+ for 12 h	232 ± 6	609 ± 25
B8	VLC-NH_4^+ for 12 h	238 ± 4	673 ± 87

The data are shown ± standard deviation, which were obtained from at least three independent experiments. HC, high-CO_2; $K_{0.5}$ (Ci), Ci concentration required for half V_{max}; VLC, very-low-CO_2; V_{max}, maximum O_2-evolving activity; WT, wild-type.

Table S4. Sequences of primers used in this study

Primer name	Sequence
For screening of insertion mutants	
aph-F1	5'-GCTTATCGATACCGTCGACCT-3'
aph-R3	5'-AACACCATCAGGTCCCTCAG-3'
RB-02	5'-GTCGACTTGGAGGATCTGGACGA-3'
LCIA-F1	5'-GACGTAGAGTAGGGCGGTTGTGTA-3'
LCIA-F2	5'-TAACGCCTCTGGCAACGTTTGTCCA-3'
LCIA-F3	5'-ATCCTTGTATGTAACGCTCGCTCTC-3'
LCIA-R1	5'-GAAGTAGGACACGCTCCAGTTCTTC-3'
LCIA-R2	5'-ATCACACCCACAACAAGACACCTG-3'
HLA3-F1	5'-GTGCCGTTTCAAAGTCAGGAACTC-3'
HLA3-F2	5'-AGCTTAAGGACCAGGATGGCCAGAA-3'
HLA3-F3	5'-CCTCTGACATCCAGAAGATCTACGA-3'
HLA3-F4	5'-TCAAGACCCCCAAGAACGCTCC-3'
HLA3-F5	5'-AAGTGCATCAAGGGCCTGTTCTC-3'
HLA3-F6	5'-GTTCACTTCATGGGCATCTACGG-3'
HLA3-F7	5'-CCTGTCCATCATTCCCCAGGAG-3'
HLA3-R1	5'-GTCATGCAGATGTAGCCCATGC-3'
HLA3-R2	5'-CTGGAACTCGTAGGTGGTGAAGAT-3'
HLA3-R3	5'-GGTGTACTTGTTCTCATCGAACTGC-3'
HLA3-R4	5'-AGGTAGATGAGGCAGTAGAAGGTGGT-3'
HLA3-R5	5'-CGCTGGTCATAGAAGACACCATC-3'
HLA3-R6	5'-CTGCTCCATCACGATGATCTTGTC-3'
HLA3-R7	5'-CTGTCACTCGTTTTCTTGCCCTAC-3'
For construction of overexpression plasmids	
LCIA-BglII-F	5'-GAAGATCTTCAAACATCTGTAGCGGCAAGTAC-3'
LCIA-EcoRI-R	5'-CGGAATTCCGTTACGCGGTGGCGGGCTTGG-3'
aph-MluI-F	5'-CGACGCGTCGACGCTGAGGCTTGACATGAT-3'
aph-R	5'-CGGGGTACCCGCTTCAAATACGC-3'
HLA3-pTY2b-IF-F	5'-AAGTCACTCGAGATCTATTGTTTGGGACTCTATCGA-3'
HLA3-pTY2b-IF-R	5'-GCTTGATATCGAATTCTTACTGGTTGCGGCCCTG-3'
LCI1-pTY2b-IF-F	5'-AAGTCACTCGAGATCTGTCGAGTACCAAGGTCCT-3'
LCI1-pTY2b-IF-R	5'-GCTTGATATCGAATTCTTACACCTTGGTGGCGCC-3'
For quantitative real-time PCR	
LCIA-qF	5'-TCTCCGTGGGAGGCAACATC-3'
LCIA-qR	5'-ACAGACCCACGGGGAACACC-3'
HLA3-qF	5'-GTGCAGCAGACCATCAAGAA-3'
HLA3-qR	5'-GACCAGCTTGGAGAACATGG-3'

LCI1-qF	5'-GCCTGACCATCTTCTTCCTG-3'
LCI1-qR	5'-TCACCATTCGCTCGTACAAA-3'
LCIB-qF	5'-CCTGATTGAGAAGGCTGTGG-3'
LCIB-qR	5'-GTAGGTCTTCAGGCCGTTGA-3'
CBLP-qF	5'-AGGTCTGGAACCTGACCAACT-3'
CBLP-qR	5'-AAGCACAGGCAGTGGATGA-3'